Multiscale Modeling of Powder Bed–Based Additive Manufacturing

Article *in* Annual Review of Materials Research · August 2016

DOI: 10.1146/annurev-matsci-070115-032158

CITATIONS
225

READS
5,319

2 authors:

Matthias Markl
Friedrich-Alexander-University of Erlangen-Nürnberg
38 PUBLICATIONS **823** CITATIONS
SEE PROFILE

Carolin Körner
Friedrich-Alexander-University of Erlangen-Nürnberg
222 PUBLICATIONS **8,334** CITATIONS
SEE PROFILE

Multi-Scale Modeling of Powder-Bed-Based Additive Manufacturing

Matthias Markl and Carolin Körner

Chair of Metals Science and Technology, Department of Materials Science, Friedrich-Alexander-Universität Erlangen-Nürnberg, Martensstr. 5, 91058 Erlangen, Germany; email: matthias.markl@fau.de

Annual Review of Materials Research
2016. 46:1–34

This article's doi:
10.1146/((please add article doi))

Keywords

additive manufacturing, selective electron beam melting, selective laser melting, lattice Boltzmann method, finite element method, cellular automaton method

Abstract

Powder bed fusion processes belong to additive manufacturing technologies which are supposed to induce the third industrial revolution. Components are built up layer-by-layer in a powder bed by selectively melting confined areas, according to sliced three dimensional model data. This technique allows manufacturing of high complex geometries hardly machinable with conventional technologies. However, the underlying physical phenomena are sparsely understood and difficult to observe during processing. Therefore, an intensive and expensive trial and error principle is applied to produce components with the desired dimensional accuracy, material characteristics and mechanical properties. This review presents numerical modeling approaches on multiple length and time scales to describe different aspects of powder bed fusion processes. In combination with tailored experiments, the numerical results enlarge the process understanding of the underlying physical mechanism and support the development of suitable process strategies and component topologies.

Contents

1. INTRODUCTION

Additive Manufacturing (AM): "a process of joining materials to make objects from 3D model data, usually layer upon layer" (1)

Additive Manufacturing (AM) designates processing technologies of component fabrication by joining materials usually layer-by-layer (1). The term itself is also referred to as 3D printing, rapid prototyping, rapid manufacturing or freeform fabrication. In media, AM is claimed to be the third industrial revolution (2). The high industrial demand is summarized in *Wohlers Report 2014*, where the market for AM, consisting of all products and services worldwide, is expected to grow from $3 billion in 2013 to more than $21 billion until 2020 (3).

The media impression and the growing industrial attention is faced with complex technologies and processes, which are yet not fully controllable, reproducible and predictable. The evolution of AM is challenged by processability and quality issues, such as premature process terminations or faults due to distortion, cracks or porosity. Assuming suitable materials, these issues are mainly addressed by the choice of process parameters, which are typically found by a trial-and-error principle until today. Besides the time consumption and expense of this procedure, the potential of AM technologies is hardly exploited.

One step towards a controllable and reproducible process is in-situ sensing and real-time control (4). The underlying correlations are gained by the combination of process observations and component analysis. Kruth et al. (5) review laser and powder-bed-based AM technologies and try to understand the physical mechanisms and interaction with the material. Although these technologies are able to process a variety of different materials, the authors state the need for further optimizations to enlarge the applicability. Newer technologies apply electron beams on metal materials, where Murr et al. (6) compare the resulting microstructure depending on the beam source. Approaches to gain further inside into the consolidation mechanism of electron beam AM technologies exceed process obser-

vations and include numerical simulations. Exemplary, Al-Bermani et al. (7) compared experimental and numerical melt pool geometries to relate them with the final microstructure. Körner, Bauereiß & Attar (8) further investigate numerical simulations and compare the results with experiments to identify the role of certain process parameters.

The physical effects occurring during AM act on multiple length and time scales. Length scales range from decimeters for residual stresses acting on complete components via micrometers for beam and powder diameters through to nanometers for the penetration depths of laser beams. Time scales cover durations from hours of a global heat treatment during manufacturing to minutes for single layer building and milliseconds of interaction time between the beam and the material. Many of these physical phenomena act on such small scales which are not covered by observation and measuring devices. Nevertheless, recognizing the interplay between these effects is crucial for a deep understanding of the process behavior and the final component quality. Therefore, modeling approaches and numerical simulations on multiple length and time scales are perfect tools to gain further insights and enable predictions by process parameter modifications suitable for further component topology optimizations.

After a short introduction into the technological concepts of powder-bed-based AM processes, the occurring physical phenomena and manufacturing issues are described. Subsequently, the two main numerical approaches on the powder scale and using a continuum approximation are discussed in detail. Issues like melt pool geometry and dynamics, porosity, surface roughness and residual stresses are considered. Additionally, extensions of these approaches to model the microstructure evolution during solidification are addressed. Finally, optimization aspects regarding the process and the component topology are considered. Based on this state of the art, future research topics are finally recommended.

2. POWDER BED FUSION PROCESSES

AM is classified by the *American Society for Testing and Materials* as one of the three pillars of manufacturing engineering technologies: additive, subtractive and forming (1). The term is defined as "a process of joining materials to make objects from 3D model data, usually layer upon layer, as opposed to subtractive manufacturing methodologies" (1). The definition covers all methods of adding material to a three dimensional physical object, but highlights that many state-of-the-art applications are layer-based approaches. Powder Bed Fusion (PBF) is one of seven AM categories and comprises all technologies applying thermal energy to partially fuse a powder bed (1).

Powder Bed Fusion (PBF): "an AM process in which thermal energy selectively fuses regions of a powder bed" (1)

2.1. Technological Concepts

Common PBF technologies are selective electron beam melting (SEBM) (9) and selective laser melting (SLM) (5, 10). A universal process chain comprises four steps: conceptualization, pre-processing, manufacturing and post-processing. After designing a component model, the next step pre-processes the model data by slicing it into several layers depending on the layer thickness and converting it to a machine conformable file format. Subsequently, the data files and process parameters are sent to the machine. The PBF manufacturing step, illustrated in **Figure 1(a)** for SLM (left) and SEBM (right), starts with preheating the current powder layer up to the processing temperature by a heater or electron beam. Secondly, the cross sections according to the component model are melted by a laser or

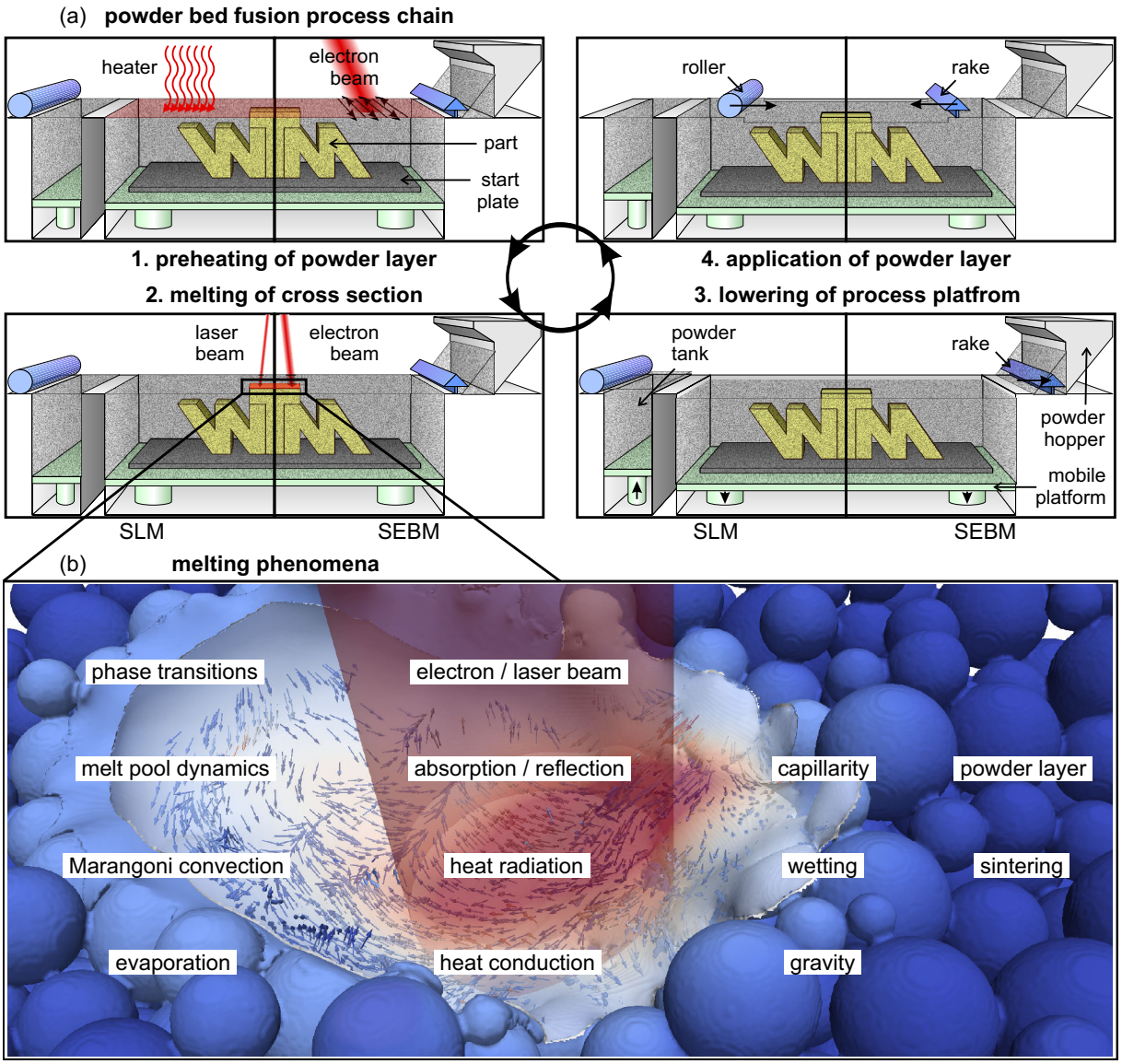

Figure 1

Principles of the PBF process chain for the SLM (left) and SEBM (right) process (a). Each layer is heated up to the preheating temperature (1) before melting the component cross section (2). Subsequently, the mobile platform is lowered about one layer thickness (3) and a new powder layer is applied before the process restarts (4). The dominant physical phenomena during melting are illustrated in a partially molten powder bed (b). The powder bed and melt pool surface are colored with the temperature distribution. Semi transparent melt pool surface enables visualization of melt pool dynamics by velocity arrows. Bottom of melt pool is visualized in white and the beam source in semi-transparent red.

electron beam. Once melting is finished, the process platform is lowered by one layer thickness. The provided powder particles by the powder tank or powder hopper are applied as a new powder layer by a roller or rake and the process restarts with preheating. At the

Table 1 Numerical models and their applied topics

Model	Application	Sec.	References
Discrete Element (DE)	powder bed generation	3	(11, 12)
Monte Carlo (MC)	beam absorption & ray tracing	3	(13–15)
Lattice Boltzmann (LB)	hydrodynamics, thermodynamics	3	(8, 16, 17)
Finite Volume (FV)	hydrodynamics, thermodynamics	3, 4	(18–21)
Finite Element (FE)	thermodynamics, mechanics	4, 6	(18, 22–25)
Phase Field (PF)	microstructure evolution	5	(26)
Cellular Automaton (CA)	grain structure evolution	5	(27–29)

end of the build process, the component has to be removed from the start plate before the component is post-processed for application purposes.

Applying lasers for melting require an additional heater for preheating but allows manufacturing in a shielding gas atmosphere under ambient pressure. The electron beam is used for preheating and melting, which restricts the material variety to electrically conducting materials and requires a vacuum inside the build chamber.

2.2. Physical Phenomena

A manifold of physical effects, visualized in **Figure 1(b)**, occur during PBF processes, which influence the process stability and the final component quality. Identifying and understanding these phenomena and their interplay is crucial for successful manufacturing. The applied numerical models on the different physical effects are summarized in **Table 1** and further described in the subsequent sections.

During heating, the powder bed is irradiated by a laser or electron beam, whereby the photon or electron energy is transformed into thermal energy by absorption. Photons are generally absorbed within the first nanometers at the surface of the material (30). In contrast to opaque continuous material, the powder bed allows deep penetration due to multiple reflections at the particle surface (30, 31). The absorbed thermal energy is distributed depending on the relative density and reflectivity of the powder bed within the top powder layers. The penetration depth of the electrons increases with increasing acceleration voltage of the electron beam gun (32). They are also deflected and scattered due to the interaction with the materials' electrons and atomic nuclei.

Thermal radiation, thermal convection and evaporation of volatile elements cause a heat loss with biquadratic, linear and exponential dependance on the building temperature, respectively. During SLM, heat convection between the material and the shielding gas occurs. Contrary, heat convection to the surrounding atmosphere is negligible during SEBM because of the vacuum in the build chamber. Due to heat conduction the absorbed thermal energy is further distributed into the material and temperature peaks at the surfaces are reduced. This effect mainly depends on the thermal diffusivity of the material and the sintering grade of the powder bed.

After preheating the base temperature of the powder bed is elevated and the single powder particles are interconnected by small sinter necks. The elevated temperature simplifies melting and reduces temperature gradients during manufacturing. The presintered powder particles act as support structures during the subsequent manufacturing and increase the thermal and electrical conductivity. Especially the electrical conductivity is crucial during SEBM for discharging (33).

During processing, the material melts and forms a melt pool. Convection depends on viscosity and is driven by different external forces like gravity, buoyancy, surface tension, capillarity, Marangoni effects or evaporation pressure. Depending on the process and the material, these phenomena have different impacts. The melt pool lifetime is commonly short, viscosities are low and gravity plays a minor role in contrast to the other forces (34). Thermal expansion induces buoyancy and exerts thermal stresses. The high surface tension in combination with the wetting ability of metals achieve a smooth surface for stable melt pools. Contrary, instable melt pools disrupt and the surface tension cause the formation of single melt balls (35–37). Marangoni forces induce fluid motion away from the temperature peak in the center of the melt pool and raise the heat transport (5, 38). Due to high melt pool temperatures the material evaporates and the resulting recoil pressures additionally drive the fluid motion. Especially in SLM processes, these pressures cause the so-called keyhole formation, where the laser beam penetrates into the material up to certain layer thicknesses forming a vapor capillary (20). Besides the convective effect, selective evaporation of volatile elements also change the local and global material composition (39).

After melting and consolidation of the material, the temperature decreases and the material solidifies. Material shrinkage during solidification induce stresses in the surrounding material which can partially relax during successive layer processing (40). The residual stresses inside the component are the main reason for distortions (10, 41).

Depending on the temperature gradients and the processing temperature, a certain microstructure evolves (39, 42, 7, 6). Due to the layer-wise manufacturing, a repeated heat treatment of the heat affected zone around the melt pool may change the microstructure by solid state phase transformations.

In the last step a new powder layer is applied, where the powder properties and the previous layer surface mainly influence the characteristics of the new powder layer. In general, a high relative density is desired, which is correlated to the flowability of the powder comprising properties like surface topology, size distribution or shape.

2.3. Manufacturing Issues

Many issues arise during PBF manufacturing regarding process stability and the quality of the final components. At beginning of each process a set of process parameters is chosen, which defines, e.g., the preheating and scanning strategy. The final component quality is often not acceptable due to defects or insufficient material properties. In the worst case, the process prematurely terminates before the component is finished.

Layer bonding defects occur due to an insufficient heat input. In this case the powder particles are not completely molten and consolidated with the bulk material and gas of the surrounding atmosphere is entrapped in the final material. Additionally, there may evolve connected channels of binding faults through many layers (43). Another source for porosity are pores inside the powder particles, which are not able to escape out of the melt pool (44).

Due to shrinkage during solidification and cooling, the dimensional accuracy especially of the first layers or overhang areas which are loosely coupled to the powder is diminished. In addition, stresses are induced during these phases as well as during the volume expansion at heating and melting (40). Causing effects are, e.g., distortion and cracks diminishing the component quality and mechanical properties (41). Delamination describes the effect, when the edges of the geometry bulge out due to residual stresses after solidification and layer bonding defects, which mainly depends on the scanning strategy and the energy input (45).

Instable melt pools cause the so-called balling effect. On the one hand, the single melt balls are formed due to the dominant surface tension exceeding the local wetting ability of the previous layer (37, 16). On the other hand, the Plateau-Rayleigh instability leads to melt pool fragmentation for length-to-width ratio larger than 2.1 (46).

Another effect mainly occurring with high energy beams is material transport (44). The maximum temperatures and evaporation rates increase and a disadvantageous constellation of melt pool lifetime, surface tension and evaporation pressure finally cause the material to accumulate at certain locations up to a height of many layer thicknesses.

In extreme cases of delamination, balling or material transport, the powder delivery system is disturbed providing further layers due to an uneven surface of the previously solidified layer. In the beginning, the resulting powder bed may show grooves, or empty spaces in the near vicinity of defects. Once the defects increase, the powder delivery system may get damaged and is not anymore able to distribute a new powder layer causing the process to terminate.

If none of these effects occur, PBF processed components achieve a flat and even top surface. SLM is often processed in the keyhole welding mode in contrast to conduction welding of SEBM, i.e., the beam drills into the material and droplets are able to leave the melt pool and splash onto the neighboring surface (37). In contrast, side walls or inclined structures exhibit surface roughness on the scale of the powder particle size (47). Therefore, SLM processes show smaller roughness values compared to SEBM due to smaller powder size distributions, layer thicknesses and beam diameters.

A highly investigated research area is the microstructure evolution during solidification and cooling, which affects most of the component's mechanical properties (42, 7, 48). Due to high melting temperatures, selective amounts of a metal alloy can evaporate and change the local material composition and also the resulting microstructure (49).

3. POWDER SCALE APPROACHES

This section focuses on numerical methods, which resolve the geometry of each single powder particle. Besides thermodynamic aspects, these models also comprise hydrodynamic effects. All numerical methods until today base on mesh approaches, where spatial resolutions on the order of micrometers are necessary to resolve the particles (16–18, 50, 51). Most of these models are explicit, which limits the time step by the Courant-Friedrich-Lewy (CFL) condition to nanoseconds in order to account for high melt pool velocities. Regardless of whether two or three dimensional models are applied, the demanding numerical effort limits the computational domain on single line or layer applications on the micro- to millimeter scale. In addition, the height of the previous layers in many simulation setups are shorter than the thermal length, which is proportional to the square root of the simulation time and the thermal diffusivity. Therefore, the bottom boundary is an active heat sink and cools the whole domain. Nevertheless, the most important hydrodynamic effects during melting and solidification, like balling, porosity or surface roughness can be studied with these domains. Therefore, the incompressible Navier-Stokes and the mass conservation equation are solved in combination with the energy conservation equation.

Many hydrodynamic effects, like wetting, capillarity and evaporation require an appropriate surface representation for surface points, normal directions and curvatures. Most of these quantities are computed by volume of fluid or level set methods. In the volume of fluid approach, each element has one value representing the amount of material inside the

element. With different algorithms, the surface representation can be approximated. Level set approaches directly store the distance and direction of the current element center point to the surface. Although the interface representation is more exact, these methods have difficulties in mass conservation.

3.1. Powder Bed Generation

During PBF manufacturing, each new layer requires the distribution of new powder particles into the build tank illustrated in Figure 1(a). In the SEBM process, the powder layer is achieved by a rake depositing particles from two powder heaps in front of two powder hoppers. Although there exists SLM machines using a rake, this technology typically applies a roller. The powder particles are provided by a separate powder tank equipped with a mobile platform. However, many powder bed approaches disregard the size distribution of the particles as well as the stochastic distribution with varying relative density by applying regularly packed powder beds of uniform size.

Körner, Attar & Heinl (16) evaluate the importance of the stochastic powder bed and apply a so-called rain drop model to generate a powder bed for two dimensional simulations. This model is also expandable to three dimensions (52). Each particle is separately placed on the previous layer, by computing the vertical location to the first contact and afterwards rotating downwards until a steady state is reached. The natural relative density with this approach is approximately 74 % or 60 % in two or three dimensions, respectively. In order to adjust it to reasonable densities between 45 % and 60 %, particles are removed until the desired packing density is reached (16). One drawback of the particle removal are unphysical holes in the powder bed, which may provoke pores or defects. Additionally, the method is disadvantageous for a parallel execution on compute clusters, which makes it less preferable for demanding three dimensional simulations.

Discrete Element (DE) Method: numerical model capable of handling individual particles of any shape in a continuous domain, where interactions are viewed as a transient problem (53)

Focusing on the influence of the final properties of the powder bed on the melting behavior, the relative density is most important (16). A simplification of the complex distribution process is to replace the rolling and raking process by a free fall discrete element (DE) model (17, 11). Each particle is able to move in a continuous space limited by boundary walls. Besides gravity forces, normal and tangential forces act on the particles during contact with each other and modify the particle motion. Cohesive and static frictional forces are neglected to achieve arbitrary packing densities. The free fall and packing process is finally interrupted once the desired relative density is reached. This model is well suited for parallelization, is very efficient and consumes only few percentages of the total computation time for PBF simulations.

Parteli (12) investigates with a DE method the behavior of complex shaped particles during powder application. Each particle is treated as a single entity but is composed of multiple spheres. Additionally, the roller and rake geometry is modeled as a moving boundary condition, driving the particles during distribution. Studies on particle interaction forces (54) reveal the crucial role of cohesive forces for the final relative density of the powder bed, which is intended to be included in the DE approach for a more realistic powder distribution simulation.

3.2. Heat Source Modeling

The temperature and its gradients are the most important quantities since many material properties, like the density, surface tension, heat conductivity, heat capacity or thermal

diffusivity are temperature dependent. These properties induce thermodynamic, hydrodynamic as well as mechanical effects, which determine the final component quality. Due to this major influence, a careful modeling of the beam as a heat source is crucial.

The heat input is divided in a horizontal intensity distribution and a vertical absorption distribution. The horizontal intensity is naturally very similar to a bell-shaped form and therefore commonly modeled by a Gaussian density function (16, 22). Efficiency factors account for energy losses for the beam control and the reflection on the material surface. The laser and electron beam show different properties regarding the length scales of their penetration depth.

For the first considerations, a bulk metal with a flat top surface is assumed. During SLM, most of the laser intensity is reflected and only a fraction is absorbed on the scale of several nanometers (55), which is commonly modeled by surface heat sources. Regarding SEBM, each electron of the beam is deflected, backscattered or absorbed once hitting the bulk material surface. Electron beams exhibit a penetration depth on the micrometer scale depending on the kinematic energy induced by the acceleration voltage of the electron beam gun and the atomic number of the material. Depending on the acceleration voltage and the atomic mass a bulb to a hemispherical shape of the affected area is formed. A suitable numerical approach to model the electron penetration into the bulk material is the Monte Carlo (MC) method. Drouin et al. (13) develop a simulation software intended to assist in interpretation of imaging and microanalysis of scanning electron microscopes. Mahale (56) applies the software ability of tracking the electron's path inside the material to estimate the absorption coefficient of different materials. But this procedure does not fully exploit the capabilities of the MC approach. It is possible to determine a full absorption profile inside the material depending on, e.g., the acceleration voltage or the inclination angle to the target surface. Klassen, Bauereiß & Körner (32) study different semi-empirical approaches to gain a phenomenological model of absorption profiles for an electron beam for different metals and compare the final model with literature values. This model as well as two approximations, which are also suitable for laser absorption, are well suited for parallel execution (57). Validating this model using the MC method opens the opportunity for further improvements and applications to other materials.

Monte Carlo (MC) Method: stochastic approach, where multiple repeated random samples approximate the solution (13)

In PBF processes the beam is able to penetrate deeper into the powder bed than into the corresponding bulk material. Photons of a laser beam are highly reflected and only a small fraction of its energy is absorbed at the particle surfaces. Therefore, the photons penetrate into the powder bed and are absorbed in deeper regions. The energy absorption is distinctively higher than the absorption coefficient of the material due to the multiple reflection. This behavior is often modeled by ray-tracing MC approaches, where the trajectories of the single photons are tracked. Wang & Kruth (14) examine such a model for the absorption during the laser sintering process of a Fe-Cu powder mixture. The authors conclude the energy absorption as crucial for numerical simulations to predict the sintering zone. A similar approach is used by Zhou, Zhang & Chen (15), where the irradiation on a bimodal powder bed is examined. The approach is validated with experimental data and is applied on the issue of balling.

3.3. Melt Pool Dynamics

Melt pool dynamics are mainly driven by capillary and Marangoni forces, evaporation pressure, and the wetting ability on the powder particles and the previous layer. Scharowsky

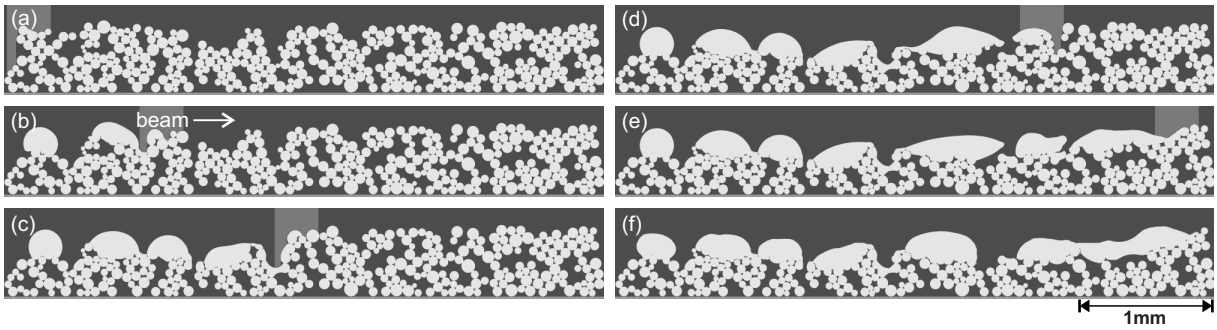

Figure 2

Temporal evolution of melt pool and balling during single line scanning in SEBM of Ti-6Al-4V with 600 W and 1.14 m/s (16). Melt pool fragments during melting and single droplets are formed.

et al. (34) observe these dynamics with a high speed camera and analyze the melt pool lifetime, size and oscillations. Numerical simulations examined by Scharowsky et al. (58) show a good agreement to high speed camera measurements.

Lattice Boltzmann (LB) Method: cellular automaton modeling discrete particle kinetics by discrete space, time, and particle velocities (63)

The underlying two dimensional numerical method has been developed by Körner, Attar & Heinl (16). It relies on a lattice Boltzmann (LB) approach (59), which is extended by free surface boundary conditions treating thermodynamics (60), surface tension, phase transitions (61) and wetting (62). They apply this model on the balling phenomenon of single scan lines during SEBM of Ti-6Al-4V. Single spot melting examples show the influence of the wetting conditions on balling, the larger the wetting angle the higher is the balling tendency. Additionally, the relative density and stochastic composition has a major influence on the melt pool geometry. **Figure 2** shows the temporal evolution of a melt pool during single line scanning with 600 W and 1.14 m/s. The balling formation is not related to a large melt pool and the Rayleigh instability, but the single droplets are directly formed during melting influenced by the local powder arrangement, wetting and capillarity.

Körner, Bauereiß & Attar (8) studies base upon these results and investigate the surface quality of SEBM manufactured vertical walls of Ti-6Al-4V as a function of scan speed, line energy and layer thickness, whereby the line energy is the ratio of beam power and scan speed. **Figure 3** illustrates the wall quality of simulations (a) and experiments (b). It increases with smaller layer thickness and higher scan speed. Higher line energies enlarge the total wall thickness. The same mechanism is responsible for beads and extrusion at the surface of the walls, which are much larger than the powder particle diameter. The interaction time of the electron beam with the material is compared to the diffusion time through one layer and an optimal scan speed is recommended. Additionally, mono particle layers are recommended, because they reduce the probability of beads and extrusion.

Further model extensions comprise the incorporation of heat radiation and evaporation (64). Comparisons of melt pool depth and width to experiments on Ti6Al4V with different beam powers and scan speeds show an excellent agreement and the melt pool temperature is limited to realistic values lower than 4000 K. However, the numerical effort in general rises by accounting for the evaporation recoil pressure due to decreased spatial resolution from 5 µm to 1 µm.

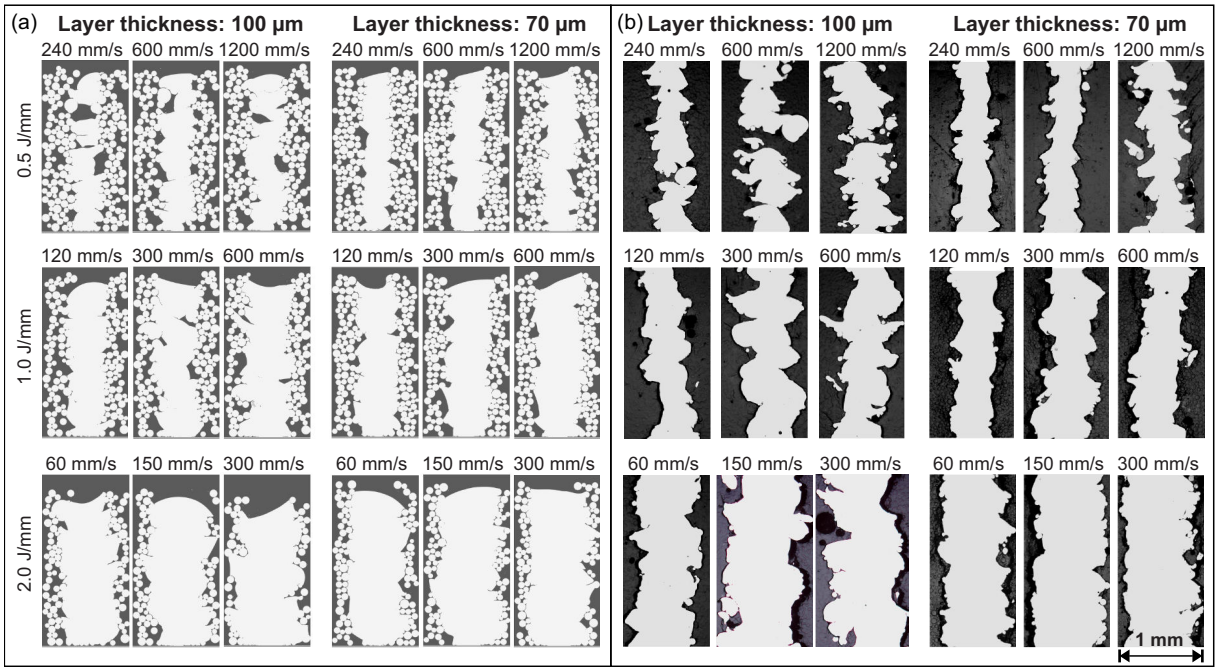

Figure 3

Comparison of wall formation of Ti-6Al-4V during SEBM as a function of scan speed, line energy and layer thickness between simulation (a) and experiment (b) (8). Increasing wall quality for smaller layer thickness and higher scan speed. Increasing wall thickness for higher line energies.

3.4. Porosity

Numerical models on the powder scale are able to predict the evolution and morphology of residual porosity within the bulk material. Different formation mechanism can be identified.

Bauereiß, Scharowsky & Körner (43) study the defect generation and propagation mechanism during SEBM applying the LB model of Körner, Attar & Heinl (16). They compare cubes of Ti6Al4V manufactured with a scan speed of 0.8 m/s and different beam powers between 90 W and 180 W with numerical results. With a beam power of 90 W, a high porosity with noticeable channels across many layers is observed, where the mechanism behind the formation is illustrated in **Figure 4**. Due to the stochastic nature of the powder bed and the insufficient melt depth, the top surface of the processed layer is uneven (layer 1 and 2). In contrast to the thermal diffusion, hydrodynamic motion driven by surface tension forces is much faster. Therefore, molten particles coalesce with neighboring solid material, which is not necessarily the previous layer. Thus, a defect is generated in layer 4 and evolves over more than ten layers. Due to the process parameters, the melt pool is not large enough to span over the defect and fill it with liquid material. Contrary, the molten particles are attracted by the defect side walls and the channel grows.

During SLM, the formation of a keyhole stabilized by vapor or plasma pressure is common. At the end of the melt pool, the keyhole collapses and is filled with liquid material. Depending on the solidification conditions, residual pores may evolve (65). Panwisawas et al. (50) report those pores for Ti-6Al-4V cubes manufactured with a laser power of 400 W

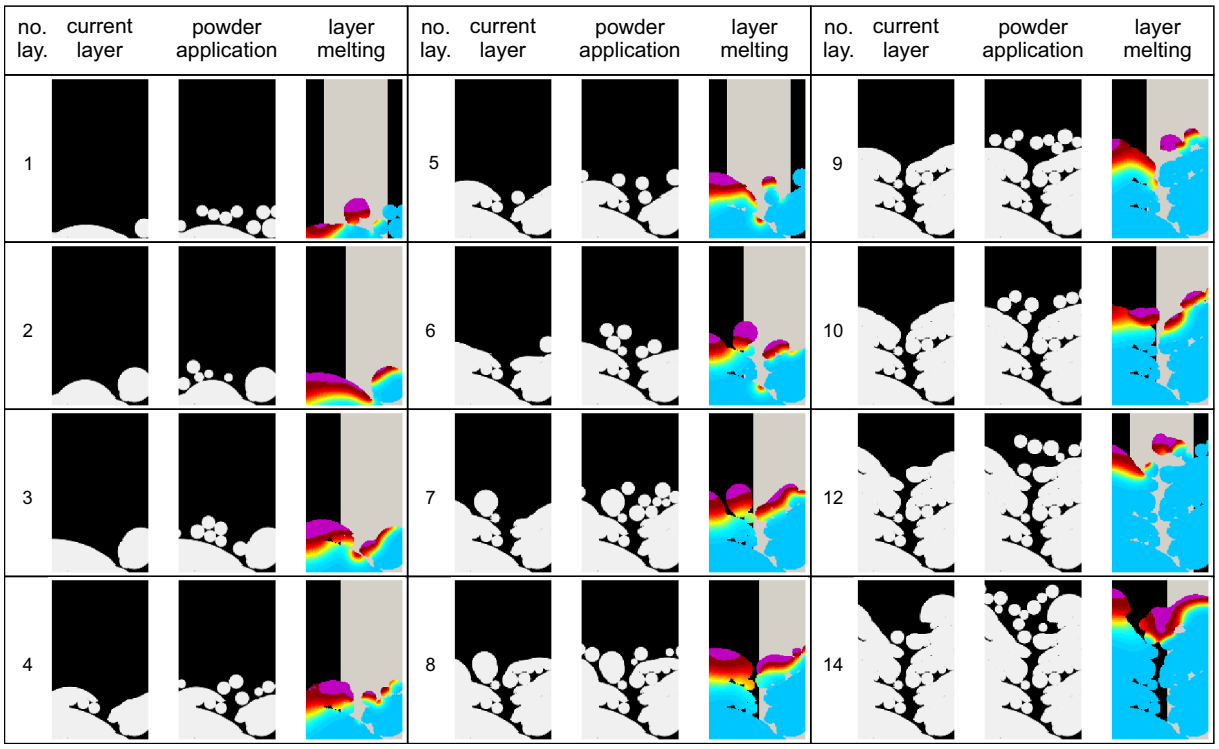

Figure 4

Evolution of a channel like fault during SEBM of Ti-6Al-4V with 90 W and 0.8 m/s over 14 layers (43). Illustrated are the current layer before (left) and after (center) powder application and the temperature distribution during melting (right), where violet regions are liquid. Capillary forces pull the liquid material out of the channel to the neighboring solid particles.

Finite Volume (FV) Method: specialized finite element method for, e.g., conservation laws computing the fluxes over the boundaries of arbitrary volumes by an integral formulation which is locally conserving (66)

and scan speeds between 2 m/s and 4.2 m/s. They apply a finite volume (FV) method and compare the melt pool motion with the resulting pore geometry. Spherical and ellipsoidal pores are found for smaller scan speeds, where the beam interacts with a small material domain. Contrary, higher scan speeds can cause the new layer to tear apart from the previous layer and form elongated pores.

3.5. Surface Roughness

Surface roughness describes small scale surface irregularities. This is a noticeable characteristic of PBF processes, since partially molten particles primarily describe the final surface topography (47). Depending on the final application, this might be beneficial, e.g., for the contact between bones and medical implants (68). With appropriate surface modifications to generate interconnected macro porosity the fixation is believed to be further improved (69). Nevertheless, in most applications surface roughness is undesirable because it weakens the mechanical properties as a source of crack initiation (70).

Strano et al. (47) investigate the surface roughness of an SLM component with different build orientations made of steel 316L. On the basis of measurements they derive a

mathematical model describing the surface roughness depending on the slope angle. They conclude that the surface roughness is sensitive on any parameter affecting the heat distribution at the surface.

Qiu et al. (71) apply an FV method (50) to study the influence of melt pool motion on the surface structure of SLM manufactured cubes of Ti6Al4V with a laser power of 400 W and scan speeds between 2 m/s and 4 m/s. They conclude the melt pool stability is most important for the surface roughness. In addition, a poor surface finish increases the possibility of channel like faults in successive layers. They identify the Marangoni forces and recoil pressures as the driving forces for melt pool instabilities. Higher scan speeds increase the melt pool surface amplifying these effects and causing melt pool splashing. The same result is observed for larger layer thicknesses, where the porosity as well as the surface roughness are highly increased.

Another FV method for SLM is applied by Gürtler et al. (51) to simulate the melt pool dynamics basing on a laser welding application (20). Therefore, the model takes evaporation and the resulting recoil pressures into account forming the keyhole. Gürtler et al. (72) further study the influence of powder distribution on the process stability. They evaluate different powder size distributions of Al-12Si-Mg and validate the resulting relative densities and thermal conductivities. Subsequently, line defects, where no particles are distributed, are introduced into the powder bed and the melt pool depth and volume are compared with 100 W and 0.75 m/s. Though, size distributions with more smaller particles are able to repair the defect slightly by smoothing the final top surface.

3.6. Three dimensional approaches

The computational effort for three dimensional simulations raises by a factor of hundred to thousand compared to two dimensional simulations. The expected computation times on simulation workstations accordingly increase from hours or days to weeks or years. These approaches require a parallel and distributed execution on compute clusters. This induces a more complex implementation task on the basis of parallel software frameworks.

Ammer et al. (17) develop a three dimensional LB method for the simulation of SEBM on Ti-6Al-4V. Besides the statistical powder bed generation, the surface tension and wetting effects and a volume heat source model (32) are taken into account. The porosity is directly measured by the known gas fraction inside the layer due to the volume of fluid approach for mass advection. These measurements are used in combination with the peak temperature to define a process window, where appropriate components are producible. Ammer et al. (73) validate the numerical results with an experimental process window (49). On the basis of this work, Markl et al. (74) investigate the process parameter optimization for higher build rates. The beam scan area as well as the line offset are modified to increase the scan speed of the electron beam. **Figure 5** illustrates the modified melt pool geometries and residual porosity during hatching of a single powder layer on bulk material when the beam crossed the simulation domain on the fifth scan line and before returning in the next scan line. Increasing the beam scan area with constant beam power and speed decreases the melt pool depth and causes porous results (c). By increasing the beam power and speed, larger melt pools reach the previous layer and are still liquid at the return of the electron beam resulting in almost no porosity (d). These results reveal the opportunity to improve scanning strategies and process parameters regarding the porosity of the final part. The approach is also successfully applied on multi-layer simulations of similar hatches (11).

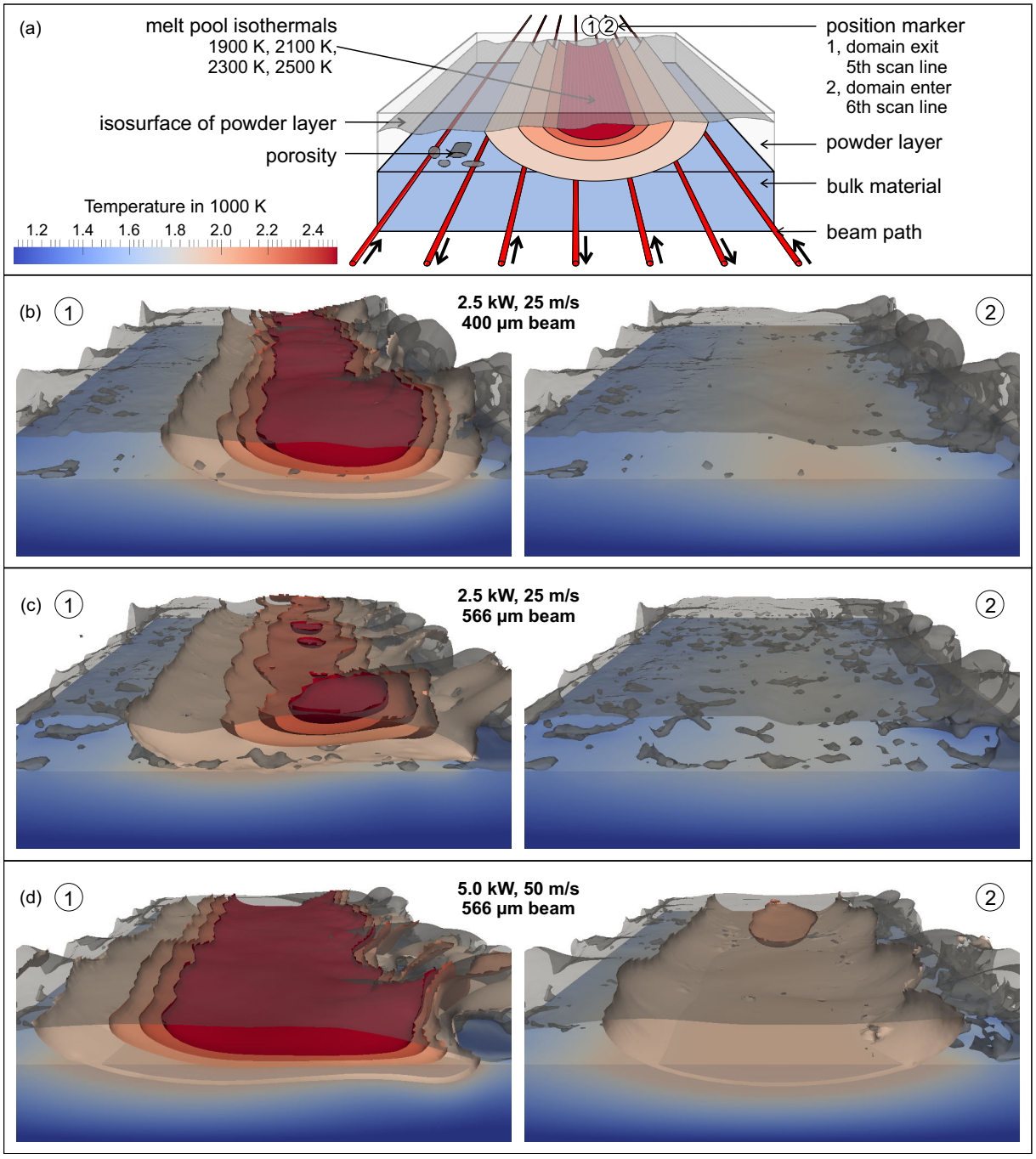

Figure 5

Melt pool geometries during SEBM hatching of one powder layer on bulk material of Ti-6Al-4V with different beam parameters (11). Sketch illustrates melt pool geometry, beam scan path, the powder layer surface and residual porosity (a). The simulation results (b-d) are taken at two beam positions on the fifth and sixth scan line.

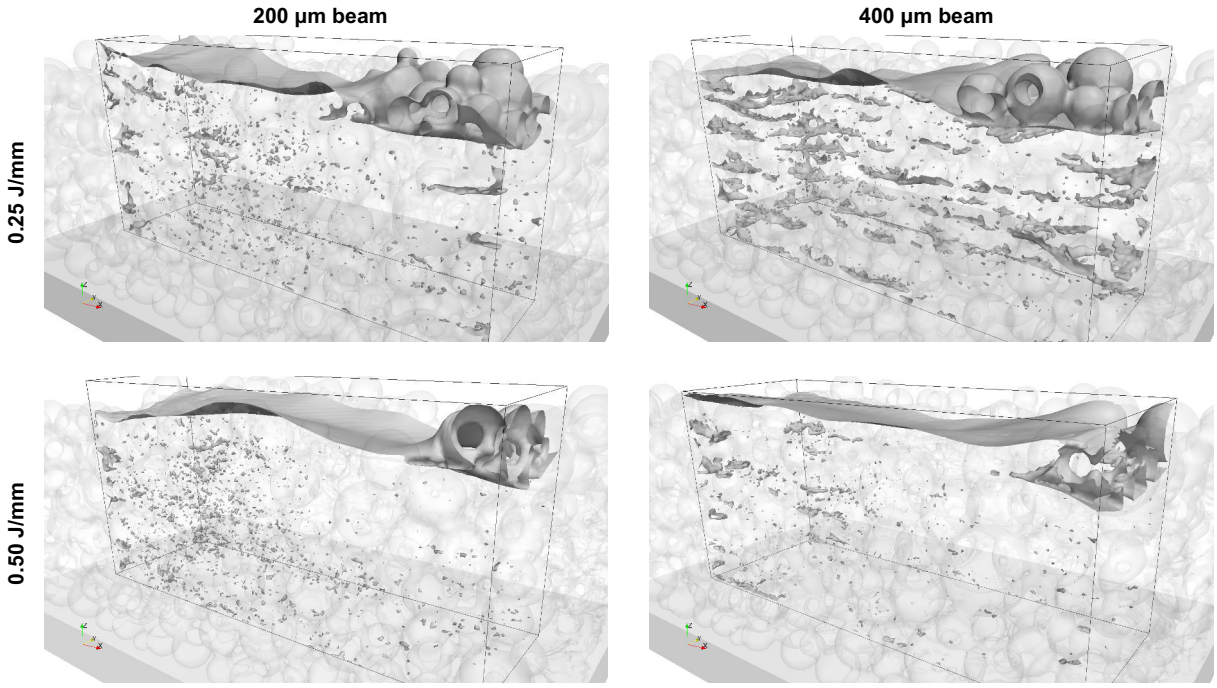

Figure 6

Multi-layer simulations of SEBM manufactured walls of Ti-6Al-4V with 150 W (27). Bulk material in light gray and isosurfaces of the top surface and interior porosity within the wall. Smaller beam sport and lower line energies do not improve the wall quality.

Markl et al. (27) further investigate with this model the quality of walls made of Ti-6Al-4V processed with a fixed beam power of 150 W and different scan speeds and beam diameters. **Figure 6** shows the numerical results of walls consisting of ten layers built with two different beam diameters and line energies. The top surface of the current melt pool and some unmolten particles are illustrated in the investigated boxes of the wall. Below, the isosurfaces represent porosity and layer bonding defects emerging from the wall boundaries. Reduced beam diameters or line energies diminish the wall quality by introducing porosity either at the beginning of the wall or as layer bonding defects at the boundaries.

Khairallah & Anderson (18) apply a Lagrangian-Eulerian approach by combining a finite element (FE) and FV method on melt pool simulations of SLM. They omit a ray tracing approach for the heat input on their stochastic powder bed of the laser and replace it by a continuous absorption model (75). They investigate single scan lines of steel 316L with 2 m/s and different beam powers between 100 W and 400 W. The melt pool always separates during melting although the length-to-width ratio is significantly changing. In contrast to the authors opinion, this melt pool fragmentation is not related to melt pool instabilities (5) but to the local stochastic of the powder bed and the melt pool geometry. The same model is applied by King et al. (76) to study overhang areas as illustrated in **Figure 7**. Severe balling occurs due to high melt pool fragmentation (a). With almost the same line energy and a smaller scan speed, a continuous track formation is achieved after the second layer (b). The smaller scan speed achieves an almost fully connected melt pool.

Finite Element (FE) Method: implicit method to solve partial differential equations by basis functions on a mesh of simple geometric elements (67)

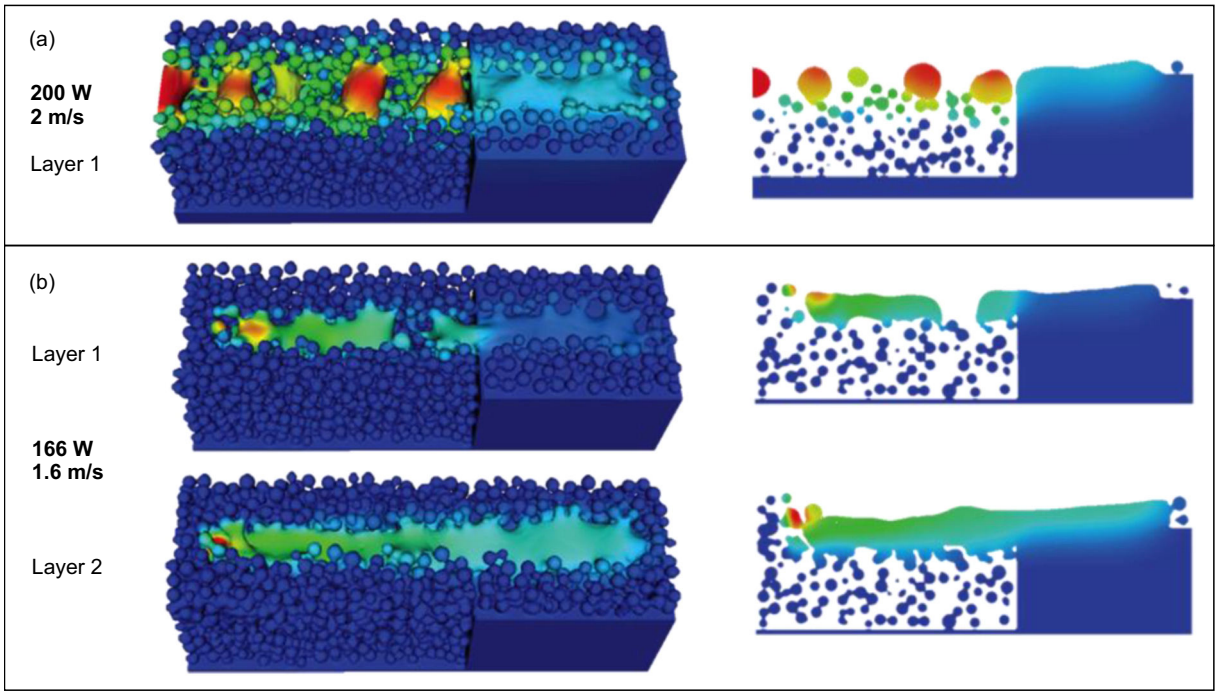

Figure 7

Melt pool geometry and temperature distribution at overhang areas produced by SLM (76). First layer in both cases is not connected due to balling. In the second layer, the track is partially remelted and finally continuous (b).

However, the model misses some crucial physical effects like Marangoni forces, evaporation or radiation. The maximum temperatures are higher than 5000 K, which is far away from physical values. Additionally, the melt pool geometry will change, when evaporation and Marangoni forces are taken into account.

4. CONTINUUM APPROACHES

Numerical grid methods representing each single particle require fine meshes. With a mean element size of approximately one tenth of the mean particle size, an appropriate representation of the interface between the material particles and the surrounding atmosphere is achieved. Regarding the SEBM process with mean particle diameters commonly larger than 50 µm a simulation domain of 1 mm^3 is represented by 8 million cubic elements with a side length of 5 µm. The corresponding computational load requires at least small scale compute clusters. For SLM processes mean powder diameters down to 10 µm are applied, where the number of cubic elements increases to 1 billion, which is only computable on large scale compute clusters. Comparing the sample domain volume of 1 mm^3 with real component dimensions, these methods are fare away from representing even small geometries.

A common approach to reduce the computational effort is to treat the powder bed as a continuum. The main advantages for a reduced computational effort are the simpler interface between material and atmosphere and the decrease of the spatial and temporal

resolution. The continuum approach omits the computation of a surface representation, including the curvature, surface tension and wetting effects, which are in general computationally demanding. Depending on further approximations of the PBF process, different time steps and minimum element sizes are required. Considering each single scan line requires as fine time steps as in mesoscopic simulations. In this case, surface and volumetric heating models are available. If the ratio of penetration depth to element size is much larger than 1, a volumetric heat source is recommended (77). However, the combination of many scan lines to scan patches or complete scan layers enable the heat input in few time steps. The minimum element size is generally restricted by the thickness of one computational layer, which can be represented by a single layer or a combination of multiple layers at once. Multi-layer simulations are often achieved by the so-called active element technique, i.e., the numerical domain is initialized with all necessary elements and only the elements corresponding to the current layers are activated. Assuming a single or combined layer thickness of 50 µm the sample volume of 1 mm^3 is represented by 8000 cubic elements, where the corresponding computational effort is attainable on single desktop computers. These modifications enable the application of larger domains up the scale of whole parts.

The continuum approach introduce a new powder phase into the numerical model, where the thermal conductivity and density are different from the bulk material (78, 79, 31). In order to compute these properties, the porosity of the powder bed is determined, which directly reveals the powder density. The thermal conductivity is then interpolated by using different functions between zero and the bulk material value depending on the porosity, e.g., a linear (24) or biquadratic (80) relation. Once the material reaches the liquidus temperature, the material properties in the affected elements are modified to bulk material. Some approaches also consider the consolidation of the material, whereby excessive elements are deleted from the model (80).

Beam scattering and intensity profiles in powder beds generated by ray tracing methods or observed by experiments are summarized in continuous models. These models neglect the lateral spread by assuming a compensation from neighboring regions and apply an intensity profile in vertical direction. Applying the absorption behavior of the compact material onto a powder bed, the relative density has to be taken into account. In the simplest approach the penetration depth is adjusted with the product of the relative density, to take the deeper penetration into account. The higher penetration due to multiple reflections of a laser beam is often modeled by exponential functions (81). A conical volumetric geometry with a linearly decreasing intensity is assumed by Shen & Chou (82). Zäh & Lutzmann (22) approximate the absorption profile by a polynomial function, where the main energy is deposited near one third of the penetration depth. A model for the absorption of a laser beam in a metal powder bed is developed by Gusarov & Kruth (31). Their model base on the radiation transfer equation and comparisons to MC approaches reveal a good accordance, except at the first micrometers the absorption is overestimated.

4.1. Melt Pool Geometry

Macroscopic studies on the melt pool geometry require primarily the solution of the heat conservation equation including the beam energy source term. Additionally, the heat sinks of thermal radiation and convection with the surrounding atmosphere for SLM is mostly covered. However, in general a flat top surface is assumed and hardly any of the following approaches consider the heat losses due to evaporation (80), which are in most cases not

negligible. Nevertheless, these models allow a rough approximation of melt pool geometries by measuring the dimensions of the isothermal at the liquidus temperature and a comparison with experimental observations (22, 83–85) or the development of closed-loop control systems (81). Increasing the numerical effort by coupling it with hydrodynamic movement improves the melt pool geometry predictions (86, 87). These models also require a flat top surface of the melt pool, whereby the applied Marangoni effect mainly drive the fluid and change the resulting melt pool dimensions and heat conduction.

Loh et al. (80) apply an FE method on SLM of single lines and investigate different melt pool geometries depending on parameter modifications for the beam power (150 W, 300 W) and scan speed (0.5 m/s, 1.14 m/s). The numerical model also includes evaporation, because the material is the aluminum alloy AA6061, where significant amounts up to 50 % of the processed layer evaporate. This effect is taken into account in combination with the thermal volume shrinkage, where the material properties in the affected elements are modified to act as atmosphere elements, i.e., the thermal conductivity in vertical and horizontal directions are elevated or lowered about certain order of magnitudes, respectively. Additionally, the density and specific heat capacity are almost set to zero, by applying the values from aluminum gas. Their corresponding numerical findings of melt pool depth and width are in accordance with experiments.

The Plateau-Rayleigh capillary instability during SLM of steel 316L, one cause for the balling effect, is studied by Gusarov et al. (46). Reducing the scan speed from 2.4 m/s to 1.2 m/s with 45 W stabilizes the process by decreasing the length-to-circumference ratio and increasing the contact area to the substrate. Experimental results are in accordance with the stability criterion and are summarized in a stability map (88). The numerical simulations of single lines are successfully applied to predict the melt pool length and circumference and the corresponding stability.

Single line and single layer simulations of steel 316L by SEBM are studied by Zäh & Lutzmann (22) using an FE method. Actually, the effects of delamination and balling are the subject of this research. However, the model only comprises thermodynamics with the dynamic electron beam as a volume source and heat radiation at the top surface. Due to the missing hydrodynamics, they evaluate different beam powers and scanning speeds and determine the length-to-width ratio in order to estimate the formation of melt balls. The best configuration with the lowest ratio is subsequently the starting point for further experimental investigations. A similar model is applied by Contuzzi, Campanelli & Ludovico (89) for simulating three successive layers of steel 316L during SLM. Although they omit heat radiation, they achieve similar melt line depths and widths for a laser beam with 100 W and 0.45 m/s.

Soylemez, Beuth & Taminger (83) also investigate the length-to-width ratio and combine it with the melt pool area. On this basis, Cheng & Chou (84) study the correlation of these two values for Ti-6Al-4V during SEBM with the process parameters of scan speed, beam diameter and power. The underlying idea is to find suitable process parameters in order to establish constant conditions during the whole built. Almost all parameter modifications have a significant influence on the inspected quantities. Of secondary significance for the length-to-width ratio are modifications of the beam power and the combination of beam diameter and scan speed. For the melt pool area the combination of beam diameter and power is of minor significance.

Ilin et al. (90) investigate manufacturing of steel 316L samples by SLM with inclined side walls by a two dimensional FE method with different parameters from 100 W to 300 W and

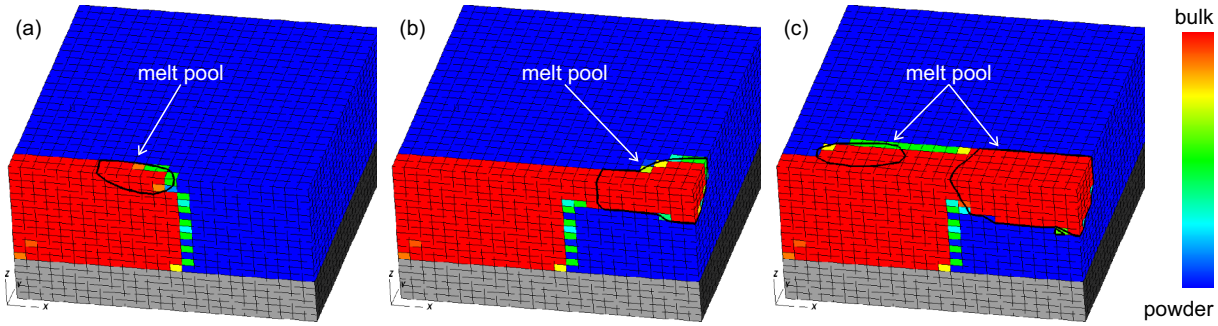

Figure 8

Melt pool geometry and relative density from powder to bulk at overhang areas for SLM of steel 316L with 167 W and 1.6 m/s, when beam enters (a), returns (b) and exits (c) the overhang area (91). Melt pool separates at the overhang area.

6 m/s to 10 m/s. Numerical simulations reveal an overheating at inclined walls, which cause balling and a bad dimensional accuracy. They develop a correction coefficient depending on the layer height of the sample, which increases the scan speed linearly up to the tenth layer by 10 % to 25 % in accordance to the inclination angle. This modification improves a continuous melt pool geometry and therefore more stable build conditions. Hodge, Ferencz & Solberg (91) study the melt pool behavior at overhang areas for SLM of steel 316L similar to King et al. (76) as illustrated in **Figure 8**. According to inclined walls, an overheating at the overhang area occurs and a separated melt pool is visible. The same strategy of reduced beam intensity can homogenize the local build conditions and improve the dimensional accuracy.

On the route to reliable and reproducible quality standards process monitoring is a crucial factor (4). Schilp et al. (81) therefore investigate mainly in a thermodynamic SLM simulation for comparisons with thermal measurements. They apply a complete model of an IN718 turbine blade into an FE approach. The geometry is transferred by the sliced representation into the mesh and the scan paths are collected to so-called load steps, where the complete scanning of one layer is combined in four load cycles. Applying several layers, temperature accumulations are detectable, which indicate regions where the scan parameters should be modified.

An FE approach in combination with an FV method is used by Jamshidinia, Kong & Kovacevic (86) to simulate the heat distribution during SEBM of Ti-6Al-4V including the hydrodynamic movement of the melt pool. Therefore, additional model assumptions are necessary, where a flat melt pool surface is the most severe. The model covers besides heat also the mass and momentum conservation, as well as frictional dissipation, buoyancy, phase transformations, radiation and Marangoni convection. The approach of Zäh & Lutzmann (22) to couple the electron beam as a heat source is applied. Melt pool dimensions of single line tracks with beam powers between 480 W and 840 W and scan speeds between 0.1 m/s and 0.5 m/s are compared with experiments and show a good agreement. Furthermore, the differences to a pure thermal model without hydrodynamics illustrated in **Figure 9** are highlighted, where deeper, narrower and hotter melt pools are predicted. Similar topics are studied by Yuan & Gu (87), where an FV method is applied on the physical mechanism during SLM of a nanocomposite, whereby the laser heat input is treated as a surface source. They further compare the influence of modifications on the laser power

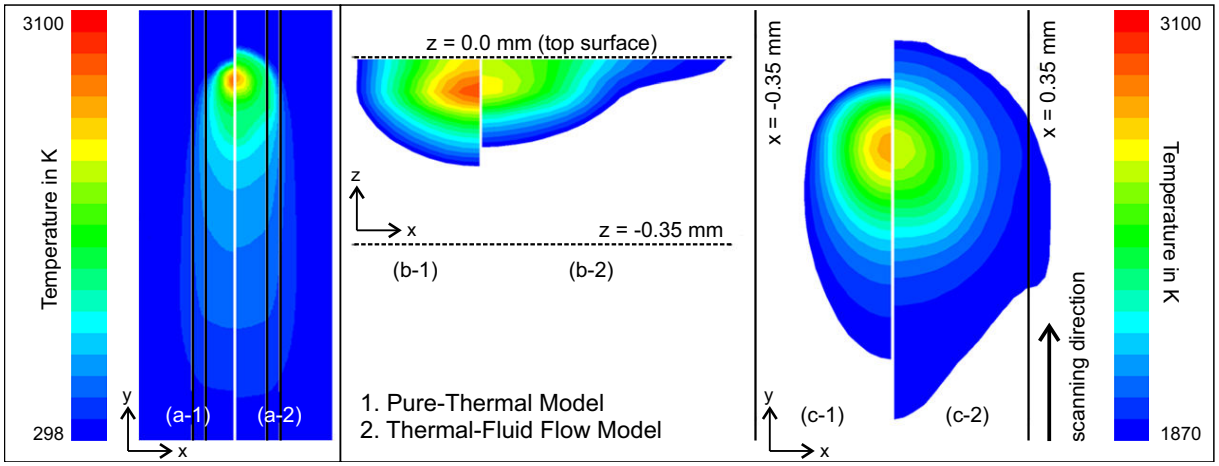

Figure 9

Melt pool comparison of SEBM for 840 W and 0.1 m/s between pure thermal (1) and thermal-fluid flow model (2) in top view (a, c) and cross section (b) (86). Fluid motion in the melt pool reduce peak temperatures and cause wider and shallower melt pool geometry.

and speed on the melt pool geometry and lifetime with experimental results on porosity, microcracks and melt ball formation.

The surface roughness is investigated by Jamshidinia & Kovacevic (92). They study the influence of different spacings between SEBM manufactured thin plates made of Ti-6Al-4V from 5 mm to 20 mm. Their FE approach (86) modeling solely the heat conduction and heat input is applied by investigating single layer experiments of melting two plates with 600 W and 0.1 m/s. During melting the distance is large enough that no interaction occurs. Contrary, after the cooling down of 5 s the maximum temperatures of the larger distances are significantly reduced. Multi-layer experiments of five successive layers reveal the same trend. In accordance to Strano et al. (47), they conclude that lower surface temperatures reduce the surface roughness. Regarding the plate spacing, this is achieved by applying the maximum distance of 20 mm.

King et al. (65) investigate keyhole mode SLM of steel 316L by applying the numerical model described by Verhaeghe et al. (93). The simulation results agree with experimental observations of melt pool geometry. Additionally, they introduce the relationship of the normalized enthalpy, which combines effects of beam power, scan speed and beam size in one quantity. They conclude for many different parameter combinations assuming a 50 µm layer thickness and a certain particle size distribution a constant threshold is suitable to distinguish between conduction and keyhole mode melting. This parameter combination into a single quantity is a desired goal to understand and predict a certain process behavior.

4.2. Residual Stress & Distortion

Remaining stresses inside a component after fabrication are called residual stresses (40). The underlying mechanism is called temperature gradient mechanism (TGM). Due to the local heat input, temperature gradients arise, the material strength decreases and the material expands. The surrounding material suppresses the expansion and once reaching the yield

strength the material is plastically deformed. During cool-down the material shrinks and induces stresses dependent on the position and solid state phase transformations.

After removal from the surrounding powder bed and the support structures, these stresses partially relax depending on the geometry and deform the final part. The geometry, the sintering degree of the surrounding powder or the size and amount of supports influence the thermal cooling behavior and have a major influence on residual stresses. In order to investigate these issues, it is necessary to model the whole component including support structures, the surrounding particle bed and the building platform.

Mercelis & Kruth (40) derive a simplified mathematical model to investigate residual stresses. Many assumptions are necessary, e.g., manufacturing at room temperature or uniform stress in each single layer. Nevertheless, this model is able to predict the described general appearance of residual stresses.

Suitable numerical methods are thermo-mechanical FE models on the macroscopic scale, where the powder bed is considered as a continuum with homogenized properties. Large temperature gradients in combination with small beam diameters and layer thicknesses cause a fine grid resolution if single melt lines are resolved (94, 95). Due to the high computational effort, approximations of the manufacturing process for complete components are common, e.g., the heat input for scan patches or complete layers, or the combination of many layers to one process step.

Early work on residual stresses during SLM has been done by Matsumoto et al. (96), where a two dimensional FE method is applied. They study the top view of melting a single layer of powder and analyze the residual stress depending on the track length. Based on these results they propose the todays state-of-the-art island scan strategy, where the whole layer is segmented into subareas with short track lengths.

Jamshidinia, Kong & Kovacevic (21) extend their numerical FV model for heat distribution (86) and couple it to an FE method to investigate residual stresses during SEBM of Ti-6Al-4V. Both models are solved simultaneously, whereby only the temperature information is exported from the FV to the FE solver. They perform single line tracks with 0.1 m/s, 0.5 m/s and 1.0 m/s and 840 W and evaluate the residual stresses during melting and after cool-down. During melting the lowest scan speed cause the highest stresses due the largest temperature gradient, whereby after cool-down the maximum stresses occur with the highest scan speed due to the highest cooling rate. Larger domain sizes covering whole components are not applicable due to the high computational effort, whereby findings from this coupling can be used to approximate better load steps for complete layers.

Li, Li & Stott (97) investigate a thermo-mechanical model, which they couple to a convection-diffusion FE method (98), to study phase changes, thermal stresses and the implication on cracks during SLM. The melt pool geometry and the location of residual stresses are related to the melt pool dynamics. Contrary, there is no dependence between the absolute residual stress values and the hydrodynamics. In order to decrease the computational effort, hydrodynamics is excluded from modeling.

Studies on residual stresses considering SLM on cubic domains are performed by Hussein et al. (24). Their simulations comprise five scan lines using a laser beam of 100 W with a scan speed of 0.1 m/s to 0.3 m/s. Their findings are in accordance to the TGM, where compressive stresses are exerted due to thermal expansion during melting. After solidification and cool-down, tensile stresses emerge due to the material shrinkage. These stresses slightly relax due to the heat treatment of neighboring scan lines, resulting in almost vanishing residual stresses perpendicular to the scan direction.

Dai & Shaw (99) investigate the manufacturing of multi-material dental restorations consisting of nickel and porcelain by SLM. Their model bases on an FE method, which is able to treat both materials, the powder shrinkage (100) as well as the thermo-mechanical evolution during the manufacturing process (101, 23). Besides the temperature gradient during single component manufacturing, the mismatch between the thermal expansion of both materials is a second source of residual stresses. The expansion coefficient of nickel is at least twice as high as that of porcelain. During solidification the material shrinkage causes high tensile and compressive stresses at the interface between nickel and porcelain, respectively. In order to reduce residual stresses to avoid cracks at the material interface, the preheating temperature or the layer thickness can be increased.

Zäh & Branner (41) investigate residual stresses and deformations of steel cantilevers during SLM. They extract the exact geometry from the manufacturing machine only with a minor modification of the support structures and the combination of 20 layers to one unit with one according load step. These simplifications require a thorough modification of the thermal input to ensure compatibility with experiments, where the main focus is set on equal temperature gradients. Besides these approximations, they regard most of the physical effects during manufacturing, like temperature dependent material properties, phase transformations, plasticity, radiation or heat conduction. They conclude with comparable residual stresses and deformations to experiments, which further allow correlation studies of the sensitivity of different process parameters (102) or the influence of support structures on residual stresses (103). Nevertheless, the simplifications cause numerical artifacts and errors, e.g., unrealistic large stress peaks. Therefore, smaller finite elements and a full layer resolution are recommended. Additionally, a pattern-based thermal load indicates a more realistic thermal behavior, especially in filigree regions (104).

Another cantilever of IN718 manufactured by SLM is investigated by Papadakis et al. (25), where similar model approximations are applied. They exploit the resulting symmetry by only simulating half of the cantilever. Three layers are combined and the thermal load is applied in one step for the whole layer. This approximation induces higher discrepancies on the final distortion in vertical than in horizontal direction (105). Therefore, their volume heat input approximation underestimate the final deformations as illustrated in **Figure 10**, whereby example simulations with a full layer resolution indicate higher residual stresses and deformations.

Keller et al. (106) develop a three dimensional FE model, which is highly simplified to allow thermo-mechanical simulations of aerospace parts. The model is further reduced by replacing the start plate by a boundary condition (107). The sliced FE meshes with a combined layer thickness of 400 µm in combination with a layer based heat input enable simulations of the complete impeller geometry. Although the numerical results indicate realistic residual stresses and distortions, an experimental validation is missing.

Due to the high computational demands of thermo-mechanical simulations, they are often restricted to few layers or combine layers to achieve whole component simulations. Nevertheless, some simulations with full-layer resolution are reported, where small components are simulated (25). Additionally, first attempts to investigate scan patterns per layer instead of whole layer heat input are made (104, 81). However, the sequential scan patterns destroy in almost all cases the process symmetry. Therefore, the whole component instead of its half with a symmetry boundary needs to be simulated, which additionally increases the computational effort. Nevertheless, the combination of both approaches can further improve residual stress and deformation predictions.

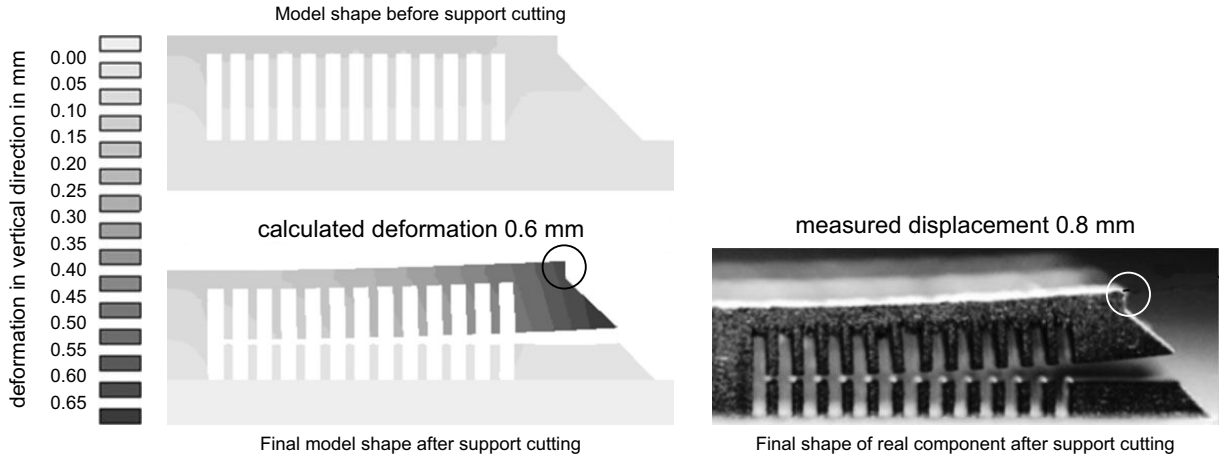

Figure 10

Distortion comparison of an SLM manufactured IN718 cantilever between simulation and experiment (105). After cutting the cantilever from the support structures, the residual stresses relax and deform the cantilever by a maximum envelope of 0.6 mm, which underestimates the experimental result of 0.8 mm.

5. MICROSTRUCTURE APPROACHES

Cellular Automaton (CA) Method: explicit mathematical idealization of a discretized physical system on a grid, where the local cell variables are modified by its neighborhood (112)

The microstructure of processed materials play an important role concerning the prediction of material thermo-mechanical properties. In continuum models there is often an isotropic material assumed. However, the layer-by-layer manufacturing of PBF processes and the corresponding solidification conditions in general cause a more or less anisotropic material. There is a broad community dealing with solidification phenomena applying mainly phase field (PF) approaches (108, 109), often modeled by FV or FE methods, and cellular automaton (CA) models (110), where Boettinger et al. (111) provides a comprehensive overview. Only few approaches combine these models with the solidification conditions of PBF processes, where a subsequent material addition, melt pool dynamics and transient temperature gradients are challenging issues.

A PF model is applied by Gong & Chou (26) to study the microstructure evolution during SEBM of Ti-6Al-4V. They investigate different undercooling conditions by different scan speed of the electron beam and conclude a faster dendrite growth for higher undercooling. The microstructure simulations mainly show multi-columnar grain growth comparable to experimental results.

Körner et al. (113) investigate tailoring the grain structure by modifying the process parameters during SEBM of IN718. Therefore, they track the direction and magnitude of the temperature gradient by numerical simulations using their LB model (8). A columnar grain structure in build direction evolves with minor gradient direction misorientations to the build direction. A modification of the line offset for hatching from 150 µm to 37.5 µm and the scan speed from 2.2 m/s to 8.8 m/s with 594 W lead to higher misorientations and cause an equiaxed grain structure. Markl et al. (27) further investigate this topic by coupling the underlying LB approach to a CA (110) method as illustrated in **Figure 11**. The model is coupled to the LB approach by interchanging the current temperature field and the phase state information. The underlying numerical concept is based on growing squares on a regular grid representing the grain geometry. Each square is allowed to grow

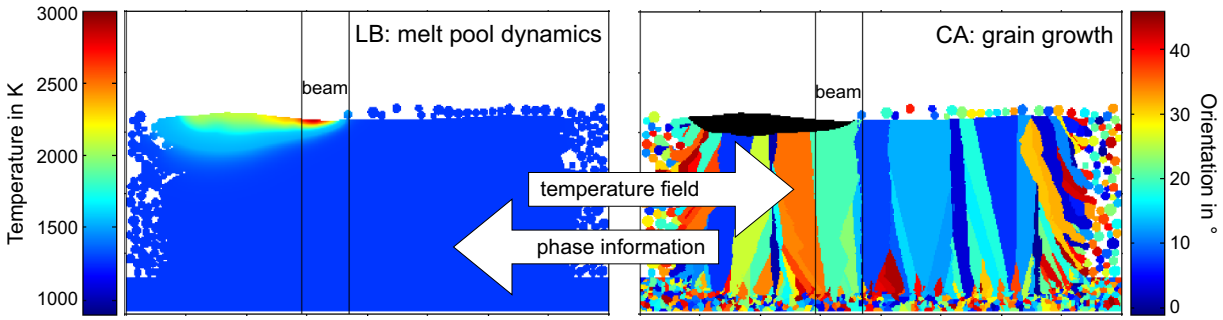

Figure 11

Coupling scheme of LB and CA approach for microstructure evolution modeling during SEBM (27). LB model provides temperature information applied for the grain growth and CA model returns current phase information to the LB model.

during solidification until it reaches all neighboring grid nodes. At each reached neighbor a new square is initialized where the growth is continuing, which is called capturing. In Figure 11, a multi-layer hatch is illustrated, where the beam and melt pool of the top layer is visible. The resulting grain structure is columnar with stray grain growth from the side surfaces. Rai, Markl & Körner (28) further investigate this topic with different melting strategies and their influence on the final grain structure.

A coupled thermal FE and CA model is applied by Zhang et al. (29) on the solidification of steel 316L, based on the CA of Rappaz & Gandin (110). Proof of concept simulations show a realistic solidification and an extension to three dimensional simulations is intended. However, experimental validation is missing.

6. OPTIMIZATION APPROACHES

In order to meet the high requirements in typical application areas as medical engineering or aerospace, the material properties as well as the topology of the components has to be optimized. Since the material properties are functions of the process parameters, the best set has to be identified. The most common approach is design of experiments (DoE), where certain sample builds are performed and the best parameter setup is interpolated depending on certain property criteria. The described numerical models are applied on exactly this optimization procedure in order to replace the majority of experiments by simulations. Once the model is validated by comparing it with sample experiments, a pre-optimization of the process parameters is possible before the first component is built. Besides the process parameters, the component itself is hardly topic of optimization research regarding AM, whereby topology and material optimization improve the overall component performance and may compensate process defects like distortion.

6.1. Process Parameter Optimization

Process parameter optimization is very complex, since many component properties are desired, e.g., porosity, crack density, dimensional accuracy, surface roughness, strength or stiffness, and a variety of material, powder and process parameters are adjustable. Therefore, expert knowledge is crucial to define a suitable parameter set for DoE. Furthermore,

most literature investigates only one to three process parameters and optimization criteria, whereby artificial intelligence approaches like neural networks are applied for interpolation.

Garg, Tai & Savalani (114) study empirical modeling of AM and apply a genetic algorithm to predict the compressive strength of final parts. The model is solely trained with experimental results and is able to identify the significant input parameters. Build time predictions by neural networks trained with experimental results are performed by Mungua, Ciurana & Riba (115). Boillat et al. (116) propose a neural network approach replacing experiments by numerical results of an FE method to optimize the production of a cylinder. They train their network to predict the radii by numerical simulations. Afterwards, the model is inverted to predict the necessary process parameters by the desired properties. The inverted model is finally applied on a greedy search, to find the local optimum. This procedure has two advantages. First, there is less expert knowledge necessary, since the initial parameters can be chosen in a wide range to train the neural network. Second, the optimization routine is automated and needs no interpretation and manual post-processing of the numerical results. This procedure allows only a few experiments starting with the best parameter set found by the limits of the FE model.

6.2. Topology & Material Optimization

Topology optimization approaches are mainly covered by FE methods, where the material distribution in the single elements is optimized. Each element is one design variable, where a solid isotropic material with penalization (SIMP) or a bidirectional evolutionary structural optimization (BESO) method is applied. The SIMP approach (117) uses a variational density for each element, which is later realized by, e.g., cellular structures in the component. Contrary, the BESO method (118) applies void-solid elements during their optimization procedure, i.e., elements are either completely filled or empty. Brackett, Ashcroft & Hague (119) presents an overview of current research areas and ideas regarding topology optimization for AM.

Khanoki & Pasini (120) apply a SIMP model for multi-objective optimization of orthopedic hip implants. The resulting functionally graded cellular material reduces the bone resorption by 76 % and the interface stress by 50 % compared to a fully dense implant.

Greifenstein & Stingl (121) develop a SIMP optimization algorithm for simultaneous material and topology optimization, which allow an efficient solution of usually complex problems. Similar approaches are applied by Mitschke et al. (122) on finding auxetic frameworks in periodic tesselations, which are further improved by a mathematical optimization process regarding the Poisson ratio (123). The non-intuitive geometry modifications realized by this optimization technique are not expected to be found by a designer and reveal the strength of automated topology optimization.

Despite process strategy improvements, high temperature gradients during PBF manufacturing will always cause residual stresses and deformations. Therefore, first ideas are to invert the final distortion and build a modified geometry (25). This approach can be nicely coupled to topology optimization methods (122, 124). At the moment, the optimized geometries are directly applied on mechanical FE models, testing different material characteristics. In the future, an intermediate step of generating the model in a macroscopic thermo-mechanical approach to get the deformed geometry including residual stresses and other properties. This route of optimization then comprises the topology as well as the applied process strategies and achieve a net-shape manufacturing.

Doubrovski, Verlinden & Geraedts (125) extend the process optimization goal by presenting an overview of current design optimization approaches, including all aspects related to the manufacturing process. They claim that knowledge on materials, computational optimization, computer aided design and simulations are separated, whereby a full design optimization needs a holistic approach.

7. CONCLUSIONS ON MULTI-SCALE MODELING

SUMMARY POINTS

1. Powder scale approaches on hydro- and thermodynamics including the most important physical effects reveal melt pool dynamics and material consolidation mechanism which are hardly gained by process observation.
2. Thermo-mechanical continuum approaches basing on process assumptions allow predictions of residual stresses and distortion for whole components.
3. Proof of concept simulations of coupled microstructure evolution approaches reveal the opportunity to tailor the final microstructure by appropriate process parameters.

Considering the manufacturing issues during PBF processes, nearly all aspects are addressed by the described numerical methods. The powder scale approaches of the FV as well as the LB method are suitable to describe the melt pool dynamics during melting and solidification in a realistic manner. For high energy inputs resulting in keyhole welding with high evaporation the resulting recoil pressures are of major importance and not negligible. To achieve also realistic melt pool temperatures it is essential to take heat radiation and evaporation into account. Manufacturing issues like balling, layer bonding defects and porosity as sources for delamination, channel faults and surface roughness are addressed.

The high computational demand of powder scale approaches is reduced by continuum approaches of the powder bed, which enables a coarsening of the spatial and temporal resolution to model complete components. Almost all thermo-mechanical models base on the FE method and simplify the manufacturing process by applying the beam energy input in few load steps. Investigated residual stresses and distortion for many different geometries reveal a general accordance to experiments. Nevertheless, the simplifications can not address the full process complexity and the final results deviate from measurements.

Only few approaches consider the microstructure evolution during PBF, whereby the CA method is well coupled to regularly meshed models. Proof-of-concept simulations reveal the most important aspects of nucleation and grain growth. This coupling allows predictions of the resulting grain structure depending on the applied process parameters.

Process optimization regarding many parameters or the topology and material of the component are also addressed. However, this is a very important topic, since especially functionally graded materials and the geometric freedom of manufacturing enables to account for, e.g., later distortions.

FUTURE ISSUES

1. Develop closed loop control mechanisms for constant and reproducible build properties and optimized components.

2. Investigate microstructure evolution including nucleation, in-situ heat treatment and solid state phase transformations.
3. Research correlations between material properties, process strategies and process optimization.

The current state of the art in PBF manufacturing operates on a predefined fixed set of process parameters. Some machines are able to modify these parameters during the build depending on the local geometry. However, there is no closed loop control mechanism, where in-situ measurements are applied to modify the current process parameters. Hu & Kovacevic (126) describe such a closed loop system for a direct laser metal powder deposition AM technology, where the powder delivery during melting is adjusted depending on measurements of the melt pool geometry. Similar approaches are conceivable for PBF processes, where fixed functions to control the scan speed are replaceable by closed-loop controllers. The necessary control functions can be gained by numerical simulations and be optimized regarding any component property like residual stress or distortion.

The combination of PBF process and microstructure simulation is hardly addressed until today. The first approaches comprise competitive grain growth depending on temperature information. Due to the melting conditions a complex microstructure evolution appears, where nucleation and stray grain formation during solidification needs to be taken into account. Depending on the processed material, the in-situ heat treatment during manufacturing of preceding layers may influence the final microstructure. Therefore, the inclusion of solid state phase transformations in numerical models is a further research topic.

In order to achieve high quality components material properties, process strategies and topology optimization is addressed. However, all numerical approaches study at most the correlation of two of these topics. A holistic investigation regarding the influence of different process strategies on material properties in a material and topology optimization routine is recommended.

DISCLOSURE STATEMENT

The authors are not aware of any affiliations, memberships, funding, or financial holdings that might be perceived as affecting the objectivity of this review.

ACKNOWLEDGMENTS

The authors would like to acknowledge funding by the German Research Foundation (DFG) within the Collaborative Research Centre 814, project B4, the Collaborative Research Centre TR103, project B2, and the Cluster of Excellence *Engineering of Advanced Materials* at the Friedrich-Alexander-Universität Erlangen-Nürnberg, and the European Union (EU) within the Clean Sky Joint undertaken under the Grant No. 326020.

LITERATURE CITED

1. ASTM F2792. 2012. Standard terminology for additive manufacturing technologies. ASTM International, West Conshohocken, PA
2. The Economist. 2012. The third industrial revolution. The Economist Newspaper Limited

3. Wohlers T, Associates W. 2014. Wohlers report 2014: 3D printing and additive manufacturing state of the industry annual worldwide progress report. Wohlers Associates

4. Mani M, Lane BM, Donmez MA, Feng SC, Moylan SP, Fesperman Jr. RR. 2015. Measurement science needs for real-time control of additive manufacturing powder bed fusion processes. Tech. rep., National Institute of Standards and Technology

5. Kruth JP, Levy G, Klocke F, Childs T. 2007. Consolidation phenomena in laser and powder-bed based layered manufacturing. *CIRP Annals - Manufacturing Technology* 56:730–759
6. Murr L, Gaytan S, Ramirez D, Martinez E, Hernandez J, et al. 2012. Metal fabrication by additive manufacturing using laser and electron beam melting technologies. *Journal of Materials Science and Technology* 28:1–14
7. Al-Bermani S, Blackmore M, Zhang W, Todd I. 2010. The origin of microstructural diversity, texture, and mechanical properties in electron beam melted Ti-6Al-4V. *Metallurgical and Materials Transactions A: Physical Metallurgy and Materials Science* 41:3422–3434
8. Körner C, Bauereiß A, Attar E. 2013. Fundamental consolidation mechanisms during selective beam melting of powders. *Modelling and Simulation in Materials Science and Engineering* 21
9. Heinl P, Rottmair A, Körner C, Singer R. 2007. Cellular titanium by selective electron beam melting. *Advanced Engineering Materials* 9:360–364
10. Gu D, Meiners W, Wissenbach K, Poprawe R. 2012. Laser additive manufacturing of metallic components: Materials, processes and mechanisms. *International Materials Reviews* 57:133–164

11. Markl M. 2015. Numerical modeling and simulation of selective electron beam melting using a coupled lattice Boltzmann and discrete element method. Ph.D. thesis, Friedrich-Alexander-Universität Erlangen-Nürnberg

12. Parteli E. 2013. DEM simulation of particles of complex shapes using the multisphere method: Application for additive manufacturing. *AIP Conference Proceedings* 1542:185–188
13. Drouin D, Couture A, Joly D, Tastet X, Aimez V, Gauvin R. 2007. Casino v2.42 - A fast and easy-to-use modeling tool for scanning electron microscopy and microanalysis users. *Scanning* 29:92–101
14. Wang X, Kruth J. 2000. Energy absorption and penetration in selective laser sintering: A ray tracing model. *Proceedings of the International Conference on Mathematical Modelling and Simulation of Metal Technologies* :673–682
15. Zhou J, Zhang Y, Chen J. 2009. Numerical simulation of laser irradiation to a randomly packed bimodal powder bed. *International Journal of Heat and Mass Transfer* 52:3137–3146

16. Körner C, Attar E, Heinl P. 2011. Mesoscopic simulation of selective beam melting processes. *Journal of Materials Processing Technology* 211:978–987

17. Ammer R, Markl M, Ljungblad U, Körner C, Rüde U. 2014. Simulating fast electron beam melting with a parallel thermal free surface lattice Boltzmann method. *Computers and Mathematics with Applications* 67:318–330
18. Khairallah S, Anderson A. 2014. Mesoscopic simulation model of selective laser melting of stainless steel powder. *Journal of Materials Processing Technology* 214:2627–2636
19. Panwisawas C, Gebelin JC, Warnken N, Broomfield R, Reed R. 2011. Numerical modelling of stress and strain evolution during solidification of a single crystal superalloy. *Advanced Materials Research* 278:204–209
20. Geiger M, Leitz KH, Koch H, Otto A. 2009. A 3D transient model of keyhole and melt pool dynamics in laser beam welding applied to the joining of zinc coated sheets. *Production Engineering* 3:127–136
21. Jamshidinia M, Kong F, Kovacevic R. 2013. The coupled CFD-FEM model of electron beam melting (EBM). *ASME District F ECTC Proceedings* 12:163–171
22. Zäh M, Lutzmann S. 2010. Modelling and simulation of electron beam melting. *Production Engineering* 4:15–23

4. Comprehensive overview of requirements for real-time control of powder bed fusion processes.

11. Comprehensive overview of three dimensional model for selective electron beam melting.

16. First numerical LB model to analyse selective beam melting processes on the powder scale.

23. Dai K, Shaw L. 2001. Thermal and stress modeling of multi-material laser processing. *Acta Materialia* 49:4171–4181
24. Hussein A, Hao L, Yan C, Everson R. 2013. Finite element simulation of the temperature and stress fields in single layers built without-support in selective laser melting. *Materials and Design* 52:638–647
25. Papadakis L, Loizou A, Risse J, Schrage J. 2014. Numerical computation of component shape distortion manufactured by selective laser melting. *Procedia CIRP* 18:90–95
26. Gong X, Chou K. 2015. Phase-field modeling of microstructure evolution in electron beam additive manufacturing. *JOM* 67:1176–1182
27. Markl M, Bauereiß A, Rai A, Körner C. 2016. Numerical investigations of selective electron beam melting on the powder scale. *Proceedings of the Fraunhofer Direct Digital Manufacturing Conference 2016*
28. Rai A, Markl M, Körner C. 2015. A coupled cellular automaton-lattice Boltzmann model for grain structure simulation during additive manufacturing. *will be submitted to Journal of Computational Materials Science*
29. Zhang J, Liou F, Seufzer W, Newkirk J, Fan Z, et al. 2013. Probabilistic simulation of solidification microstructure evolution during laser-based metal deposition. *24th International SFF Symposium - An Additive Manufacturing Conference, SFF 2013* :739–748
30. Tolochko N, Laoui T, Khlopkov Y, Mozzharov S, Titov V, Ignatiev M. 2000. Absorptance of powder materials suitable for laser sintering. *Rapid Prototyping Journal* 6:155–160
31. Gusarov A, Kruth JP. 2005. Modelling of radiation transfer in metallic powders at laser treatment. *International Journal of Heat and Mass Transfer* 48:3423–3434
32. Klassen A, Bauereiß A, Körner C. 2014. Modelling of electron beam absorption in complex geometries. *Journal of Physics D: Applied Physics* 47
33. Eschey C, Lutzmann S, Zäh M. 2009. Examination of the powder spreading effect in electron beam melting (EBM). *20th Annual International Solid Freeform Fabrication Symposium, SFF 2009* :308–319
34. Scharowsky T, Osmanlic F, Singer R, Körner C. 2014. Melt pool dynamics during selective electron beam melting. *Applied Physics A: Materials Science and Processing* 114:1303–1307
35. Tolochko N, Mozzharov S, Yadroitsev I, Laoui T, Froyen L, et al. 2004. Balling processes during selective laser treatment of powders. *Rapid Prototyping Journal* 10:78–87
36. Yadroitsev I, Bertrand P, Smurov I. 2007. Parametric analysis of the selective laser melting process. *Applied Surface Science* 253:8064–8069
37. Yadroitsev I, Gusarov A, Yadroitsava I, Smurov I. 2010. Single track formation in selective laser melting of metal powders. *Journal of Materials Processing Technology* 210:1624–1631
38. Louvis E, Fox P, Sutcliffe C. 2011. Selective laser melting of aluminium components. *Journal of Materials Processing Technology* 211:275–284
39. Das S. 2003. Physical aspects of process control in selective laser sintering of metals. *Advanced Engineering Materials* 5:701–711
40. Mercelis P, Kruth JP. 2006. Residual stresses in selective laser sintering and selective laser melting. *Rapid Prototyping Journal* 12:254–265
41. Zäh M, Branner G. 2010. Investigations on residual stresses and deformations in selective laser melting. *Production Engineering* 4:35–45
42. Murr L, Quinones S, Gaytan S, Lopez M, Rodela A, et al. 2009. Microstructure and mechanical behavior of Ti-6Al-4V produced by rapid-layer manufacturing, for biomedical applications. *Journal of the Mechanical Behavior of Biomedical Materials* 2:20–32
43. Bauereiß A, Scharowsky T, Körner C. 2014. Defect generation and propagation mechanism during additive manufacturing by selective beam melting. *Journal of Materials Processing Technology* 214:2522–2528
44. Vandenbroucke B, Kruth J. 2007. Selective laser melting of biocompatible metals for rapid manufacturing of medical parts. *Rapid Prototyping Journal* 13:196–203

28. Comprehensive numerical model on the powder scale to analyze microstructure evolution during additive manufacturing.

40. Excellent physical and mathematical background on residual stresses.

41. Comparison of numerical and experimental SLM manufactured cantilever stresses and distortion.

45. Zäh M, Kahnert M. 2009. The effect of scanning strategies on electron beam sintering. *Production Engineering* 3:217–224
46. Gusarov A, Yadroitsev I, Bertrand P, Smurov I. 2007. Heat transfer modelling and stability analysis of selective laser melting. *Applied Surface Science* 254:975–979
47. Strano G, Hao L, Everson R, Evans K. 2013. Surface roughness analysis, modelling and prediction in selective laser melting. *Journal of Materials Processing Technology* 213:589–597
48. Kruth JP, Badrossamay M, Yasa E, Deckers J, Thijs L, Van Humbeeck J. 2010. Part and material properties in selective laser melting of metals. *16th International Symposium on Electromachining, ISEM 2010* :3–14
49. Jüchter V, Scharowsky T, Singer R, Körner C. 2014. Processing window and evaporation phenomena for Ti-6Al-4V produced by selective electron beam melting. *Acta Materialia* 76:252–258
50. Panwisawas C, Qiu C, Sovani Y, Brooks J, Attallah M, Basoalto H. 2015. On the role of thermal fluid dynamics into the evolution of porosity during selective laser melting. *Scripta Materialia* 105:14–17
51. Gürtler FJ, Karg M, Leitz KH, Schmidt M. 2013. Simulation of laser beam melting of steel powders using the three-dimensional volume of fluid method. *Physics Procedia* 41:881–886
52. Shi Y, Zhang Y. 2008. Simulation of random packing of spherical particles with different size distributions. *Applied Physics A: Materials Science and Processing* 92:621–626
53. Cundall PA, Strack ODL. 1979. Discrete numerical model for granular assemblies. *Geotechnique* 29:47–65
54. Parteli E, Schmidt J, Blümel C, Wirth KE, Peukert W, Pöschel T. 2014. Attractive particle interaction forces and packing density of fine glass powders. *Scientific Reports* 4
55. Fischer P, Romano V, Weber H, Karapatis N, Boillat E, Glardon R. 2003. Sintering of commercially pure titanium powder with a Nd:YAG laser source. *Acta Materialia* 51:1651–1662
56. Mahale TR. 2009. Electron beam melting of advanced materials and structures. Ph.D. thesis, North Carolina State University
57. Markl M, Ammer R, Ljungblad U, Rüde U, Körner C. 2013. Electron beam absorption algorithms for electron beam melting processes simulated by a three-dimensional thermal free surface lattice Boltzmann method in a distributed and parallel environment. *Procedia Computer Science* 18:2127–2136
58. Scharowsky T, Bauereiß A, Singer R, Körner C. 2012. Observation and numerical simulation of melt pool dynamic and beam powder interaction during selective electron beam melting. *23rd Annual International Solid Freeform Fabrication Symposium - An Additive Manufacturing Conference, SFF 2012* :815–820
59. Körner C, Pohl T, Rüde U, Thürey N, Zeiser T. 2006. In *Numerical Solution of Partial Differential Equations on Parallel Computers*, eds. A Bruaset, A Tveito, vol. 51 of *Lecture Notes in Computational Science and Engineering*. Springer Berlin Heidelberg, 439–466
60. Markl M, Körner C. 2015. Free surface Neumann boundary condition for the advection-diffusion lattice Boltzmann method. *Journal of Computational Physics* 301:230–246
61. Attar E, Körner C. 2011. Lattice Boltzmann model for thermal free surface flows with liquid-solid phase transition. *International Journal of Heat and Fluid Flow* 32:156–163
62. Attar E, Körner C. 2009. Lattice Boltzmann method for dynamic wetting problems. *Journal of Colloid and Interface Science* 335:84–93
63. Chen S, Doolen G. 1998. Lattice Boltzmann method for fluid flows. *Annual Review of Fluid Mechanics* 30:329–364
64. Klassen A, Scharowsky T, Körner C. 2014. Evaporation model for beam based additive manufacturing using free surface lattice Boltzmann methods. *Journal of Physics D: Applied Physics* 47
65. King W, Barth H, Castillo V, Gallegos G, Gibbs J, et al. 2014. Observation of keyhole-

47. Excellent physical and mathematical background on surface roughness.

mode laser melting in laser powder-bed fusion additive manufacturing. *Journal of Materials Processing Technology* 214:2915–2925
66. Eymard R, Gallouët T, Herbin R. 2000. Finite volume methods. *Handbook of Numerical Analysis* 7:713–1018
67. Szabo B, Babuška I. 1991. Finite element analysis. A Wiley-Interscience publication. John Wiley & Sons
68. Deligianni D, Katsala N, Ladas S, Sotiropoulou D, Amedee J, Missirlis Y. 2001. Effect of surface roughness of the titanium alloy Ti-6Al-4V on human bone marrow cell response and on protein adsorption. *Biomaterials* 22:1241–1251
69. Heinl P, Müller L, Körner C, Singer R, Müller F. 2008. Cellular Ti-6Al-4V structures with interconnected macro porosity for bone implants fabricated by selective electron beam melting. *Acta Biomaterialia* 4:1536–1544
70. Cansizoglu O, Harrysson O, Cormier D, West H, Mahale T. 2008. Properties of Ti-6Al-4V non-stochastic lattice structures fabricated via electron beam melting. *Materials Science and Engineering A* 492:468–474
71. Qiu C, Panwisawas C, Ward M, Basoalto H, Brooks J, Attallah M. 2015. On the role of melt flow into the surface structure and porosity development during selective laser melting. *Acta Materialia* 96:72–79
72. Gürtler FJ, Karg M, Dobler M, Kohl S, Tzivilsky I, Schmidt M. 2014. Influence of powder distribution on process stability in laser beam melting: Analysis of melt pool dynamics by numerical simulations. *25th International SFF Symposium - An Additive Manufacturing Conference, SFF 2014* :1099–1117
73. Ammer R, Rüde U, Markl M, Jüchter V, Körner C. 2014. Validation experiments for LBM simulations of electron beam melting. *International Journal of Modern Physics C* 25
74. Markl M, Ammer R, Rüde U, Körner C. 2015. Numerical investigations on hatching process strategies for powder-bed-based additive manufacturing using an electron beam. *International Journal of Advanced Manufacturing Technology* 78:239–247
75. Gusarov A, Yadroitsev I, Bertrand P, Smurov I. 2009. Model of radiation and heat transfer in laser-powder interaction zone at selective laser melting. *Journal of Heat Transfer* 131:1–10
76. King W, Anderson A, Ferencz R, Hodge N, Kamath C, Khairallah S. 2015. Overview of modelling and simulation of metal powder bed fusion process at Lawrence Livermore National Laboratory. *Materials Science and Technology (United Kingdom)* 31:957–968
77. Li J, Li L, Stott F. 2004. Comparison of volumetric and surface heating sources in the modeling of laser melting of ceramic materials. *International Journal of Heat and Mass Transfer* 47:1159–1174
78. Rombouts M, Froyen L, Gusarov A, Bentefour E, Glorieux C. 2005. Photopyroelectric measurement of thermal conductivity of metallic powders. *Journal of Applied Physics* 97
79. Gusarov A, Kovalev E. 2009. Model of thermal conductivity in powder beds. *Physical Review B - Condensed Matter and Materials Physics* 80
80. Loh LE, Chua CK, Yeong WY, Song J, Mapar M, et al. 2014. Numerical investigation and an effective modelling on the selective laser melting (SLM) process with aluminium alloy 6061. *International Journal of Heat and Mass Transfer* 80:288–300
81. Schilp J, Seidel C, Krauss H, Weirather J. 2014. Investigations on temperature fields during laser beam melting by means of process monitoring and multiscale process modelling. *Advances in Mechanical Engineering* 2014
82. Shen N, Chou K. 2012. Thermal modeling of electron beam additive manufacturing process - Powder sintering effects. *ASME 2012 International Manufacturing Science and Engineering Conference Collocated with the 40th North American Manufacturing Research Conference and in Participation with the Int. Conf., MSEC 2012* :287–295
83. Soylemez E, Beuth J, Taminger K. 2010. Controlling melt pool dimensions over a wide range of

76. Multi-scale overview of three dimensional numiercal models for powder bed fusion.

material deposition rates in electron beam additive manufacturing. *21st Annual International Solid Freeform Fabrication Symposium - An Additive Manufacturing Conference, SFF 2010* :571–582

84. Cheng B, Chou K. 2013. Melt pool geometry simulations for powder-based electron beam additive manufacturing. *24th International SFF Symposium - An Additive Manufacturing Conference, SFF 2013* :644–654
85. Childs T, Hauser G, Badrossamay M. 2005. Selective laser sintering (melting) of stainless and tool steel powders: Experiments and modelling. *Proceedings of the Institution of Mechanical Engineers, Part B: Journal of Engineering Manufacture* 219:339–357
86. Jamshidinia M, Kong F, Kovacevic R. 2013. Numerical modeling of heat distribution in the electron beam melting of Ti-6Al-4V. *Journal of Manufacturing Science and Engineering, Transactions of the ASME* 135
87. Yuan P, Gu D. 2015. Molten pool behaviour and its physical mechanism during selective laser melting of TiC/AlSi10Mg nanocomposites: Simulation and experiments. *Journal of Physics D: Applied Physics* 48
88. Gusarov A, Smurov I. 2010. Modeling the interaction of laser radiation with powder bed at selective laser melting. *Physics Procedia* 5:381–394
89. Contuzzi N, Campanelli S, Ludovico A. 2011. 3D finite element analysis in the selective laser melting process. *International Journal of Simulation Modelling* 10:113–121
90. Ilin A, Logvinov R, Kulikov A, Prihodovsky A, Xu H, et al. 2014. Computer aided optimisation of the thermal management during laser beam melting process. *Physics Procedia* 56:390–399
91. Hodge N, Ferencz R, Solberg J. 2014. Implementation of a thermomechanical model for the simulation of selective laser melting. *Computational Mechanics* 54:33–51
92. Jamshidinia M, Kovacevic R. 2014. The influence of heat accumulation on the surface roughness in additive manufacturing by electron beam melting (EBM). *Proceedings - ASPE 2014 Spring Topical Meeting: Dimensional Accuracy and Surface Finish in Additive Manufacturing* :45–50
93. Verhaeghe F, Craeghs T, Heulens J, Pandelaers L. 2009. A pragmatic model for selective laser melting with evaporation. *Acta Materialia* 57:6006–6012
94. Riedlbauer D, Steinmann P, Mergheim J. 2014. Thermomechanical finite element simulations of selective electron beam melting processes: Performance considerations. *Computational Mechanics* 54:109–122
95. Shen N, Chou K. 2012. Simulations of thermo-mechanical characteristics in electron beam additive manufacturing. *ASME International Mechanical Engineering Congress and Exposition, Proceedings (IMECE)* 3:67–74
96. Matsumoto M, Shiomi M, Osakada K, Abe F. 2002. Finite element analysis of single layer forming on metallic powder bed in rapid prototyping by selective laser processing. *International Journal of Machine Tools and Manufacture* 42:61–67
97. Li J, Li L, Stott F. 2004. Thermal stresses and their implication on cracking during laser melting of ceramic materials. *Acta Materialia* 52:4385–4398
98. Li J, Li L, Stott F. 2004. A three-dimensional numerical model for a convection-diffusion phase change process during laser melting of ceramic materials. *International Journal of Heat and Mass Transfer* 47:5523–5539
99. Dai K, Shaw L. 2006. Parametric studies of multi-material laser densification. *Materials Science and Engineering A* 430:221–229
100. Dai K, Shaw L. 2005. Finite element analysis of the effect of volume shrinkage during laser densification. *Acta Materialia* 53:4743–4754
101. Dai K, Shaw L. 2004. Thermal and mechanical finite element modeling of laser forming from metal and ceramic powders. *Acta Materialia* 52:69–80
102. Krol T, Seidel C, Zäh M. 2013. Prioritization of process parameters for an efficient optimisation of additive manufacturing by means of a finite element method. *Procedia CIRP* 12:169–174

103. Krol T, Seidel C, Schilp J, Hofmann M, Gan W, Zäh M. 2013. Verification of structural simulation results of metal-based additive manufacturing by means of neutron diffraction. *Physics Procedia* 41:849–857
104. Seidel C, F. Zäh M, Wunderer M, Weirather J, A. Krol T, Ott M. 2014. Simulation of the laser beam melting process - Approaches for an efficient modelling of the beam-material interaction. *Procedia CIRP* 25:146–153
105. Papadakis L, Loizou A, Risse J, Bremen S, Schrage J. 2014. A computational reduction model for appraising structural effects in selective laser melting manufacturing. *Virtual and Physical Prototyping* 9:17–25
106. Keller N, Neugebauer F, Xu H, Ploshikhin V. 2013. Thermo-mechanical simulation of additive layer manufacturing of titanium aerospace structures. *Proceedings of the DGM International Congress on Light Materials 2013*
107. Neugebauer F, Keller N, Xu H, Kober C, Ploshikhin V. 2014. Simulation of selective laser melting using process specific layer based meshing. *Proceedings of the Fraunhofer Direct Digital Manufacturing Conference 2014*
108. Boettinger W, Warren J, Beckermann C, Karma A. 2002. Phase-field simulation of solidification. *Annual Review of Materials Science* 32:163–194
109. Chen LQ. 2002. Phase-field models for microstructure evolution. *Annual Review of Materials Science* 32:113–140
110. Rappaz M, Gandin CA. 1993. Probabilistic modelling of microstructure formation in solidification processes. *Acta Metallurgica Et Materialia* 41:345–360
111. Boettinger W, Coriell S, Greer A, Karma A, Kurz W, et al. 2000. Solidification microstructures: Recent developments, future directions. *Acta Materialia* 48:43–70
112. Wolfram S. 1983. Statistical mechanics of cellular automata. *Reviews of Modern Physics* 55:601–644
113. Körner C, Helmer H, Bauereiß A, Singer R. 2014. Tailoring the grain structure of IN718 during selective electron beam melting. *MATEC Web of Conferences* 14
114. Garg A, Tai K, Savalani M. 2014. State-of-the-art in empirical modelling of rapid prototyping processes. *Rapid Prototyping Journal* 20:164–178
115. Mungua J, Ciurana J, Riba C. 2009. Neural-network-based model for build-time estimation in selective laser sintering. *Proceedings of the Institution of Mechanical Engineers, Part B: Journal of Engineering Manufacture* 223:995–1003
116. Boillat E, Kolossov S, Glardon R, Loher M, Saladin D, Levy G. 2004. Finite element and neural network models for process optimization in selective laser sintering. *Proceedings of the Institution of Mechanical Engineers, Part B: Journal of Engineering Manufacture* 218:607–614
117. Bendsoe M, Sigmund O. 2003. Topology optimization: Theory, methods, and applications. Engineering Online Library. Springer Berlin Heidelberg
118. Querin O, Steven G, Xie Y. 1998. Evolutionary structural optimisation (ESO) using a bidirectional algorithm. *Engineering Computations (Swansea, Wales)* 15:1031–1048
119. Brackett D, Ashcroft I, Hague R. 2011. Topology optimization for additive manufacturing. *22nd Annual International Solid Freeform Fabrication Symposium - An Additive Manufacturing Conference, SFF 2011* :348–362
120. Khanoki S, Pasini D. 2011. Multiscale design and multiobjective optimization of orthopaedic cellular hip implants. *Proceedings of the ASME Design Engineering Technical Conference* 5:935–944
121. Greifenstein J, Stingl M. 2014. Simultaneous material and topology optimization based on topological derivatives. *IFIP Advances in Information and Communication Technology* 443:118–127
122. Mitschke H, Schwerdtfeger J, Schury F, Stingl M, Körner C, et al. 2011. Finding auxetic frameworks in periodic tessellations. *Advanced Materials* 23:2669–2674

123. Schwerdtfeger J, Wein F, Leugering G, Singer R, Körner C, et al. 2011. Design of auxetic structures via mathematical optimization. *Advanced Materials* 23:2650–2654
124. Chahine G, Smith P, Kovacevic R. 2010. Application of topology optimization in modern additive manufacturing. *21st Annual International Solid Freeform Fabrication Symposium - An Additive Manufacturing Conference, SFF 2010* :606–618
125. Doubrovski Z, Verlinden J, Geraedts J. 2011. Optimal design for additive manufacturing: Opportunities and challenges. *Proceedings of the ASME Design Engineering Technical Conference* 9:635–646
126. Hu D, Kovacevic R. 2003. Sensing, modeling and control for laser-based additive manufacturing. *International Journal of Machine Tools and Manufacture* 43:51–60